

# We are IntechOpen, the world's leading publisher of Open Access books Built by scientists, for scientists

6,900

Open access books available

186,000

International authors and editors

200M

Downloads

Our authors are among the

154

Countries delivered to

TOP 1%

most cited scientists

12.2%

Contributors from top 500 universities



WEB OF SCIENCE™

Selection of our books indexed in the Book Citation Index  
in Web of Science™ Core Collection (BKCI)

Interested in publishing with us?  
Contact [book.department@intechopen.com](mailto:book.department@intechopen.com)

Numbers displayed above are based on latest data collected.  
For more information visit [www.intechopen.com](http://www.intechopen.com)



## Un-Cooled Microbolometers with Amorphous Germanium-Silicon ( $a\text{-Ge}_x\text{Si}_y\text{:H}$ ) Thermo-Sensing Films

Mario Moreno<sup>1</sup>, Alfonso Torres<sup>1</sup>, Roberto Ambrosio<sup>2</sup> and Andrey Kosarev<sup>1</sup>

<sup>1</sup>*National Institute of Astrophysics, Optics and Electronics, INAOE,*

<sup>2</sup>*Universidad Autonoma de Ciudad Juarez, UACJ,*

*Mexico*

### 1. Introduction

Silicon integrated circuits (IC) in conjunction with the micro-machining technology for thin films, have opened new ways for the development of low cost and reliable night vision systems based on thermal detectors. Among the thermal detectors used as pixels on IR focal plane arrays, the microbolometer appears as one of them. A microbolometer is a device in which the IR transduction is performed through a change in the resistivity of its thermo-sensing material, due to the heating effect caused by the absorbed radiation. Among the requirements for the materials used as thermo-sensing layer in microbolometers it can be mentioned a high activation energy ( $E_a$ ), high temperature coefficient of resistance (TCR), low noise, and compatibility with standard CMOS fabrication processes. A variety of materials have been used as thermo-sensing elements in microbolometers, as vanadium oxide ( $\text{VO}_x$ ) (B. E. Cole, 1998, 2000), metals (A. Tanaka, 1996), polycrystalline (S. Sedky, 1998) and amorphous semiconductors (A. J. Syllaios, 2000).

Those materials have shown good characteristics but also some disadvantages.  $\text{VO}_x$  has a moderated value of TCR ( $0.021 \text{ K}^{-1}$ ) and low resistivity, however it is not a standard material in the IC technology. Metals as titanium are compatible with the standard IC technology, have low resistivity but also have very low TCR values. Polycrystalline semiconductors have high TCR values ( $0.05 \text{ K}^{-1}$ ) and moderated resistivity, however they are deposited at relatively high temperatures ( $700 - 900 \text{ }^\circ\text{C}$ ), which results in an incompatibility with a microbolometer fabrication post-process on a silicon wafer surface, containing an readout integrated circuit (ROIC).

Recently, it has been reported the study of W-doped  $\text{VO}_2$  (H. Takami, 2011) which has a TCR of above  $0.1 \text{ K}^{-1}$ , and low resistivity values. However, this material is not standard on Si CMOS microelectronics facilities. GaAs/AlGaAs heterojunction bolometers (P.K.D.D.P. Pitigala, 2011) also have been reported, which have demonstrated TCR values of  $0.04 \text{ K}^{-1}$ . However those structures are very complex, since they are fabricated with 30 periods of GaAs/ $\text{Al}_{0.57}\text{Ga}_{0.43}\text{As}$  junctions.

Hydrogenated amorphous silicon ( $a\text{-Si:H}$ ) is a mature material on the microelectronics and photovoltaic industries. For un-cooled microbolometers  $a\text{-Si:H}$  is very attractive to be used

as thermo-sensing material, since intrinsic a-Si:H has a very large activation energy ( $E_a$ ) of above 1 eV, and therefore, provide a very large thermal coefficient of resistance (TCR) of  $0.13 \text{ K}^{-1}$ . However intrinsic a-Si:H has a very low room temperature conductivity ( $\sigma_{\text{RT}} \leq 1 \times 10^{-9} (\Omega\text{cm})^{-1}$ ), resulting in a very high pixel resistance when is used as thermo sensing material in microbolometers ( $R_{\text{pixel}} \geq 10^9 \Omega$ ). Such high pixel resistance causes a mismatch with the input impedance of the CMOS ROIC. For commercial microbolometers, boron doping is commonly used in order to decrease the undesirable resistivity of intrinsic a-Si:H (A. J. Syllaios, 2000), to values of pixel resistance of around  $30 \times 10^6 \Omega$ , however it also results on a reduction on the activation energy ( $E_a \approx 0.22 \text{ eV}$ ) and on the TCR ( $-0.028 \text{ K}^{-1}$ ), and therefore in a decrement on the pixel performance.

In our work we have studied the electrical and optical properties of amorphous germanium-silicon (a- $\text{Ge}_x\text{Si}_y\text{:H}$ ) and amorphous germanium-silicon-boron (a- $\text{Ge}_x\text{Si}_y\text{B}_z\text{:H}$ ) thin films deposited by plasma (PECVD) (R. Ambrosio, 2004; A. Kosarev, 2006; A. Torres, 2008; M. Moreno, 2007, 2008, 2010). Intrinsic a- $\text{Ge}_x\text{Si}_y\text{:H}$  has better performance characteristics than a-Si:H,B when is used as thermo-sensing element, since it has a high activation energy ( $E_a = 0.37 \text{ eV}$ ), a high TCR ( $\alpha = -0.047 \text{ K}^{-1}$ ), a moderated room temperature conductivity ( $\sigma_{\text{RT}} \approx 6 \times 10^{-5} (\Omega\text{cm})^{-1}$ ), and therefore a moderated pixel resistance ( $R_{\text{pixel}} \approx 30 \times 10^7 \Omega$ ) (M. Moreno, 2007, 2008) when is used as thermo sensing element in microbolometers.

In the other hand a- $\text{Ge}_x\text{Si}_y\text{B}_z\text{:H}$  has an improved room temperature conductivity ( $\sigma_{\text{RT}} \approx 10^{-2} - 10^{-3} (\Omega\text{cm})^{-1}$ ), and therefore a moderated pixel resistance ( $R_{\text{pixel}} \approx 1 - 5 \times 10^6 \Omega$ ) (M. Moreno, 2007, 2008), but also it has a low activation energy ( $E_a \approx 0.18 - 0.22 \text{ eV}$ ) and low the TCR ( $-0.023 - 0.028 \text{ K}^{-1}$ ).

In this chapter we present a summary on the study of a- $\text{Ge}_x\text{Si}_y\text{:H}$  and a- $\text{Ge}_x\text{Si}_y\text{B}_z\text{:H}$  thin films and their application as thermo-sensing element in microbolometers. We have fabricated, characterized and studied two devices configurations labeled as planar (the standard configuration used in commercial microbolometer arrays) and sandwich structures. The later shows several advantages when intrinsic materials are used as thermo-sensing element. Finally we studied the performance characteristics of the different device configurations and compared them with commercial devices and those reported on literature.

## 2. Principle of operation of un-cooled microbolometers

The operation of a microbolometer is based on the temperature rise of the thermo-sensing material by the absorption of the incident IR radiation. The change in temperature causes a change on its electrical resistance, which is measured by an external circuit. Microbolometers based on amorphous semiconductors have advantages over other types of thermal detectors, including microbolometers that use other kind of thermo-sensing materials. The advantages are mainly technological, since these microbolometers are fully compatible with silicon CMOS fabrication technology, there is no need of additional fabrication equipment in a IC production line. Are relatively of simple fabrication and can be processed at relatively low temperature by PECVD. The above make them ideal for a post-process fabrication over a CMOS read-out circuit.

Fig. 1 shows a scheme of one microbolometer (B. E. Cole, 1998); it is built on a membrane usually made of  $\text{SiN}_x$ . Over the membrane is deposited the thermo-sensing material and the IR absorber material. The membrane provides thermal isolation to the thermo-sensing film.

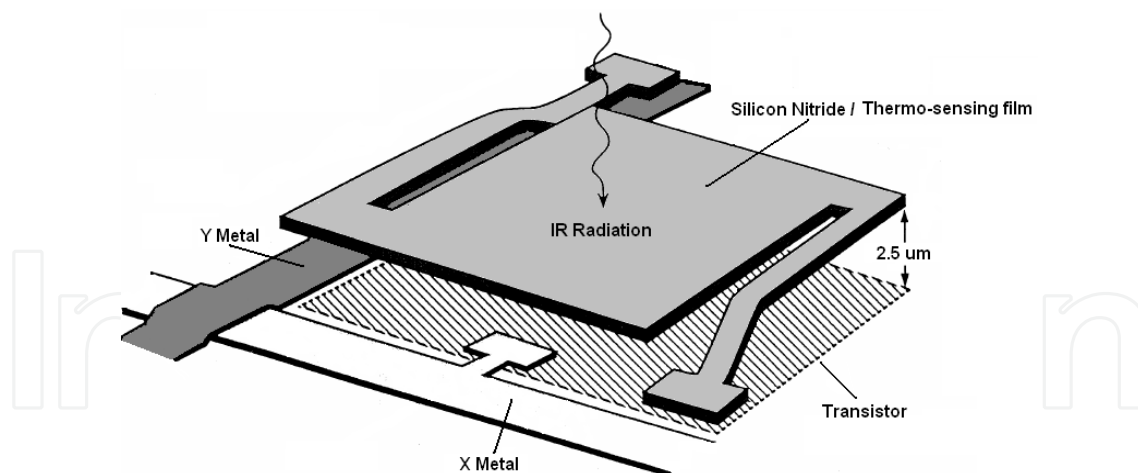


Fig. 1. Microbolometer scheme.

## 2.1 Thermal insulation

There are three mechanisms of heat transfer that occur in a thermal detector, they are conduction, convection and radiation. Conduction mechanisms occur when the heat flows from the thermo-sensing area along the supporting legs to the substrate. Conduction is critical when the pixels are very close, since the heat can flow from one pixel to a neighbor pixel. Convection occurs when the heat flows in the presence of a surrounding atmosphere, this mechanism is not very important if the detector is encapsulated in a vacuum package. Radiation mechanism is presented by the fact that the detector radiates to its surroundings and the surroundings radiate to it.

When the microbolometers are encapsulated in an evacuated package, with an IR transmitting window, convection and radiation mechanisms are minimized. Thus the main loss of heat mechanism is conduction from the thermo-sensing material to the substrate through the supporting structure.

The supporting structure is a very important part of thermal detectors, it provides three functions, mechanical support, electrical conducting path and thermal conducting path. In order to avoid heat losses in microbolometers, it is necessary to improve the thermal insulation. In microbolometers there are two main thermal insulation configurations: single-level and two-level configurations.

Single level configuration consists in depositing a membrane over the silicon (Si) substrate and after that, opening a hole in the Si substrate, employing bulk micromachining techniques. Bulk micromachining consumes area, since the Si substrate is etched with a side wall angle of 54.9 degrees. The electronic circuit (which forms part of the read out circuit) is fabricated next to the pixel, consuming area also. That results in a 20% fill factor.

The two-level configuration allows the fabrication of the electronics circuit in the substrate and after that, the fabrication of the microbolometer in a low temperature post process over the electronics, by using surface micromachining techniques. With this configuration is saved substrate area, achieving a fill factor of above 70%.

In order to fabricate thermal sensors in a post process, over a wafer surface, containing an IC circuit; it is necessary to use low temperatures during the fabrication process. By employing

Plasma Enhanced Chemical Vapor deposition (PECVD) it is possible to deposit thin films at relatively low temperatures (150 - 350 °C).

## 2.2 Infrared absorber films

An absorber element is a very important part in un-cooled IR microbolometers, its role is based in the absorption of IR radiation and the transfer of heat to the thermo-sensing material. The main requirements of absorbing materials for un-cooled microbolometers are: A high absorbance coefficient in the range  $\lambda = 8 - 12 \mu\text{m}$ , simple fabrication and compatibility with the silicon CMOS technology.

The IR absorption can be improved employing a resonant micro-cavity, where the thermo-sensing film is separated from the substrate by a gap equivalent to one quarter of the wavelength at which it will be operating. A mirror (Al or Ti) is deposited over the substrate surface, under the thermo-sensing material. In this configuration the radiation that was not absorbed by the thermo-sensing film will resound inside the cavity and will be re-absorbed by the thermo-sensing element.

Terrestrial objects have temperatures around of 300K, with IR emission centered in 10  $\mu\text{m}$ . Thus un-cooled microbolometers employed for detection of objects at room temperature, should have a gap from the substrate of 2.5  $\mu\text{m}$ , for the fabrication of the resonant micro-cavity.

Several materials have been employed as absorbing films in microbolometers, which are deposited over the thermo-sensing film. Among the most employed are some metals, as black gold film (M. Hirota, 1998), which has a very high absorption coefficient of IR radiation (more than 90 %), however it is not a standard material in CMOS technology.  $\text{SiN}_x$  films are employed commonly as absorber films in microbolometers (A. Schaufelbühl, 2001, S. Sedky, 1998), since its absorption coefficient can be tuned by the deposition parameters and it is a standard material in CMOS technology.

## 2.3 Thermo-sensing films

The thermo-sensing material is perhaps the most important element in a microbolometer. The increment in temperature in the sensing material causes a change in some temperature-dependent parameter. In the case of a microbolometer that parameter is the resistance.

The thermo-sensing material should have a large temperature coefficient of resistance, TCR ( $\alpha(T)$ ), which is defined by Eq. 1, where  $E_a$  is the activation energy,  $K$  is the Boltzman constant and  $T$  is temperature.

$$\alpha(T) = (1/R)[dR/dT] \approx E_a / KT^2 \quad (1)$$

A large TCR means that a small change in temperature in the sensing material will result in a large change in resistance. Eq. 1 shows that the TCR and  $E_a$  are directly related, thus a high  $E_a$  in the material is needed.

For un-cooled microbolometers vanadium oxide,  $\text{VO}_x$ , was the first thermo-sensing element employed (B. E. Cole, 1998), since it has a moderated TCR,  $\alpha(T) \approx 0.021 \text{ K}^{-1}$ , however it is not a standard material in silicon CMOS technology. Some metals have been employed also,

which are compatible with Si-CMOS technology, however they have low values of TCR (Pt,  $\alpha(T) \approx 0.0015 \text{ K}^{-1}$ ).

Hydrogenated amorphous silicon (a-Si:H) prepared by PECVD is very attractive to be used as thermo-sensing film in microbolometers, for room temperature operation (A. J. Syllaios, 2000). It is compatible with the IC technology, has a high activation energy,  $E_a \approx 0.8 - 1 \text{ eV}$  and high value of TCR,  $\alpha(T) \approx 0.1 - 0.13 \text{ K}^{-1}$ , however it also has a very high undesirable resistivity, which often cause a mismatch with the input impedance of the read-out circuits. In order to reduce the a-Si:H high resistance, boron doping has been employed. The B doped a-Si:H films have a significant reduction in its resistivity, however a reduction in  $E_a$  and TCR is obtained also,  $E_a \approx 0.22 \text{ eV}$  and  $\text{TCR} \approx 0.028 \text{ K}^{-1}$  (A. J. Syllaios, 2000).

Material	TCR (K <sup>-1</sup> )	E <sub>a</sub> (eV)	$\sigma_{RT} (\Omega \text{ cm})^{-1}$	Reference
VO <sub>x</sub>	0.021	0.16	$2 \times 10^{-1}$	B. E. Cole, 1998
a-Si:H (PECVD)	0.1 - 0.13	0.8-1	$\sim 1 \times 10^{-9}$	A. J. Syllaios, 2000
a-Si:H,B (PECVD)	0.028	0.22	$5 \times 10^{-3}$	A. J. Syllaios, 2000
a-Ge <sub>x</sub> Si <sub>y</sub> :H (PECVD)	0.043	0.34	$1.6 \times 10^{-6}$	M. Moreno, 2008
Poly-SiGe	0.024	0.18	$9 \times 10^{-2}$	S. Sedky, 1998
Ge <sub>x</sub> Si <sub>1-x</sub> O <sub>y</sub>	0.042	0.32	$2.6 \times 10^{-2}$	E. Iborra, 2002
YBaCuO	0.033	0.26	$1 \times 10^{-3}$	J. Delerue, 2003

Table 1. Common materials employed as thermo-sensing films in microbolometers.

In our work (R. Ambrosio, 2004; A. Kosarev, 2006; A. Torres, 2008; M. Moreno, 2007, 2008, 2010), amorphous germanium-silicon, a-Ge<sub>x</sub>Si<sub>y</sub>:H, deposited by PECVD has been studied as thermo-sensing films in un-cooled microbolometer, obtaining high activation energy,  $E_a = 0.34 \text{ eV}$ , consequently a high value of  $\text{TCR} = 0.043 \text{ K}^{-1}$  and improved but still high resistivity.

Table 1 shows the most common materials employed as thermo-sensing films in microbolometers. As can be seen in the table, there are available several materials which can be used as thermo-sensing films. Intrinsic amorphous silicon, a-Si:H and a-Ge<sub>x</sub>Si<sub>y</sub>:H, show the largest TCR values and are fully compatible with the silicon CMOS technology, however they have also the smallest values of room temperature conductivity,  $\sigma_{RT}$ .

### 3. Main figures of merit of un-cooled microbolometers

In this section the different figures of merit of a microbolometer, as thermal characteristics, responsivity and detectivity are presented. The different types of noise in microbolometer are described also.

#### 3.1 Thermal capacitance, C<sub>th</sub>, thermal conductance, G<sub>th</sub> and thermal response time, τ<sub>th</sub>

A simple representation of a microbolometer is shown in Fig. 2, the detector has a thermal capacitance, C<sub>th</sub>, and it is coupled to the substrate which is a heat sink, by a thermal conductance, G<sub>th</sub>.

When the detector receives modulated IR radiation, the rise in temperature is found by solving the balance equation, Eq. 2; where C<sub>th</sub> (expressed in JK<sup>-1</sup>) is the thermal capacitance of the supporting membrane containing the thermo sensing film, while G<sub>th</sub> (expressed in WK<sup>-1</sup>) is the thermal conductance of the legs, which is considered the main heat loss

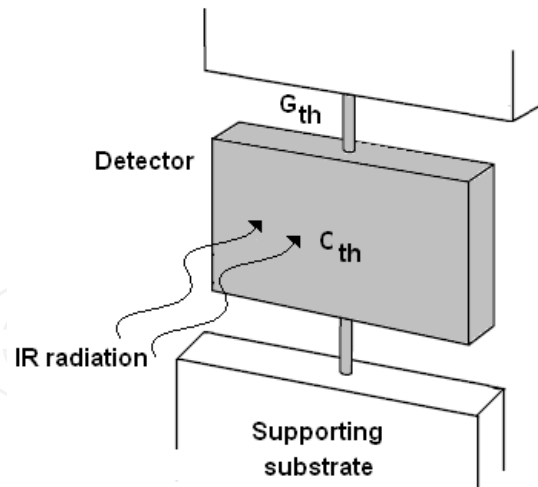


Fig. 2. Microbolometer representation.

mechanism.  $\Delta T$  is the temperature difference of the hot and reference junctions.  $A_{cell}$  is the detector area,  $\beta$  is the fill factor, which is the ratio of the thermo-sensing film area to the total cell area,  $\eta$  is the optical absorption coefficient, defined as the fraction of the radiant power falling on the thermo-sensing area, which is absorbed by that area.  $P_0$  is the intensity of the IR modulated radiation,  $\omega$  is the angular modulation frequency and  $t$  is time [2.6].

$$C_{th} d(\Delta T) / dt + G_{th} (\Delta T) = \eta \beta A_{cell} P_0 \exp(j\omega t) \quad (2)$$

The solution of the balance equation is shown in Eq. 3:

$$\Delta T = \eta \beta A_{cell} P_0 / G_{th} (1 + \omega^2 \tau_{th}^2)^{1/2} \quad (3)$$

Where,  $\tau_{th}$  (expressed in seconds) is the thermal response time of the microbolometer, it is defined by Eq. 4, which establishes a relation between  $\tau_{th}$ ,  $C_{th}$  and  $G_{th}$ . Typical values of thermal time constant are in the range of milliseconds, which are much longer than the typical time of photon detectors.

$$\tau_{th} = C_{th} / G_{th} \quad (4)$$

For unmodulated radiation Eq. 3 can be reduced to:

$$\Delta T(\omega = 0) = \eta \beta A_{cell} P_0 / G_{th} \quad (5)$$

Eq. 5 shows that the increment of temperature,  $\Delta T$ , in the detector is inversely proportional to the thermal conductance  $G_{th}$  of its legs. In order to achieve a high performance microbolometers  $\Delta T$  should be as high as possible and therefore  $G_{th}$  as small as possible, which can be done by making very thin the detector legs.

### 3.2 Responsivity

Responsivity,  $R$ , is defined as the ratio of the pixel output signal to the incident radiant power (in Watts) falling on the pixel (P. W. Kruse, 2001). The output signal is an electrical signal that can be voltage or current, thus  $R$  can be expressed in Volts/Watts (voltage

responsivity,  $R_u$ ) or Amps/Watts (current responsivity,  $R_I$ ). In order to obtain  $R$ , we can use the simplest model, where it is assumed that there is no heating due the electrical bias in the detector (Joule heating), and also it is assumed a constant electrical bias to the detector.

When the microbolometer is current biased, the output signal is voltage,  $V_s$ , given by Eq. 6, where  $I_b$  is the bias current,  $R_{cell}$  is the electrical resistance of the microbolometer,  $\alpha$  is the TCR, described by Eq. 1 and  $\Delta T$  is the increment of temperature in the detector, obtained in Eq. 5.

$$V_s = I_b R_{cell} \alpha \Delta T \quad (6)$$

Voltage responsivity,  $R_v$ , is obtained by combining equations 3 and 6, and dividing by  $P_o A_{cell}$ , which is the incident radiant power, the result is shown in Eq. 7.

$$R_v = \eta \beta I_b \alpha R_{cell} / G_{th} (1 + \omega^2 \tau_{th}^2)^{1/2} \quad (7)$$

$$R_v = \eta \beta I_b \alpha R_{cell} / G_{th} \quad (8)$$

For unmodulated radiation,  $\omega = 0$ , Eq. 7 is simplified in Eq. 8, which is the DC responsivity. When the microbolometer is voltage biased equations 7 and 8 are transformed to Eq. 9 and Eq. 10 respectively, where  $R_I$  is current responsivity.

$$R_I = \eta \beta V_b \alpha / G_{th} R_{cell} (1 + \omega^2 \tau_{th}^2)^{1/2} \quad (9)$$

$$R_I = \eta \beta V_b \alpha / G_{th} R_{cell} \quad (10)$$

### 3.3 Noise in microbolometers

There are four main sources of noise in microbolometers (P. W. Kruse, 2001), which are Johnson noise, 1/f noise, temperature fluctuation noise and background fluctuation noise, these noise types are uncorrelated and are described in the following subsections.

#### 3.3.1 Johnson noise

The Johnson noise component,  $V_j$ , is described by Eq. 11, where  $k$  is the Boltzmann constant,  $T_{cell}$  is the bolometer temperature,  $R_{cell}$  is the bolometer resistance and  $\Delta f$  is the bandwidth of the integration time.

$$V_j = (4k T_{cell} R_{cell} \Delta f)^{1/2} \quad (11)$$

#### 3.3.2 1/f noise

The 1/f noise is characterized by a spectrum that depends inversely on frequency and is described by Eq. 12, where  $V$  is the product of the bias current -  $I_b$  and the electrical resistance of the microbolometer -  $R_{cell}$ ,  $f$  is the frequency at which the noise is measured and  $n$  is the 1/f noise parameter, which depend on the material detector.

$$V_{1/f} = \left( V^2 n / f \right)^{1/2} \quad (12)$$

1/f noise is the dominant noise at low frequencies and falls below the Johnson noise at higher frequencies, the transition is commonly called the “knee”.

### 3.3.3 Temperature fluctuation noise

A thermal detector which is in contact with its environment (by conduction and radiation), exhibits random fluctuations in temperature, since the interchange of heat with its surrounding has a statistical nature; this is known as temperature fluctuation noise. The mean square temperature fluctuation noise voltage is given by Eq. 13 (P. W. Kruse, 2001).

$$V_{TF}^2 = \left( 4kT_{cell}^2 \Delta f / G \left( 1 + \omega^2 \tau_{th}^2 \right)^{1/2} \right) V^2 \alpha^2 \quad (13)$$

### 3.3.4 Background fluctuation noise

When the heat exchange by conduction between the detector and its surroundings is negligible, in comparison with the radiation exchange, the temperature fluctuation noise will be identified as background fluctuation noise.

The mean square background fluctuation noise is given by Eq. 14, where  $T_{cell}$  is the detector temperature and  $T_B$  is the background temperature.

$$V_{BF}^2 = 8 A_{cell} \eta \sigma k \left( T_{cell}^5 + T_B^5 \right) R_{cell}^2 \quad (14)$$

The total noise voltage is obtained by adding the 4 noise contributions as is shown in Eq. 15.

$$V_N^2 = V_J^2 + V_{1/f}^2 + V_{TF}^2 + V_{BF}^2 \quad (15)$$

## 3.4 Detectivity

Detectivity,  $D^*$  (expressed in  $\text{cmHz}^{1/2}\text{Watt}^{-1}$ ), is a figure of merit for all types of detectors, it is defined as the pixel output signal to noise ratio per unit of incident radiant power falling on the detector, measured in a 1 Hz bandwidth. In other words,  $D^*$  is the normalized signal to noise ratio in the detector and is shown in Eq. 16.

$$D^* = \left( R_V \left( A_{cell} \Delta f \right)^{1/2} \right) / V_N \quad (16)$$

In Eq. 16  $R_v$  is the voltage responsivity,  $A_{cell}$  is the detector area,  $\Delta f$  is the frequency bandwidth and  $V_N$  is the contribution of the four noises. It is clear that in order to achieve a high  $D^*$  the responsivity should be as high as possible and the noise as small as possible.

The fundamental limit to sensitivity of any thermal detector is set by random fluctuations in the temperature of the detector due to fluctuations in the radiant power exchange between the detector and its surroundings. The highest possible value of  $D^*$  of a thermal detector operated at room temperature is  $D^* = 1.98 \times 10^{10} \text{ cmHz}^{1/2}\text{W}^{-1}$  (A. Rogalski, 2003).

#### 4. Amorphous germanium-silicon (a-Ge<sub>x</sub>Si<sub>y</sub>:H) and germanium-silicon-boron alloys (a-Ge<sub>x</sub>Si<sub>y</sub>B<sub>z</sub>:H)

Intrinsic amorphous silicon (a-Si:H) prepared by PECVD is a very attractive material to be used in microbolometers as thermo-sensing film. It has a high activation energy,  $E_a \approx 0.8 - 1$  eV and high value of temperature coefficient of resistance, TCR,  $\alpha(T) \approx 0.1 - 0.13 \text{ K}^{-1}$ , however it also has a high undesirable resistivity.

Amorphous germanium-silicon (a-Ge<sub>x</sub>Si<sub>y</sub>:H) films deposited by PECVD have been studied as thermo-sensing film in microbolometers (R. Ambrosio, 2004; A. Kosarev, 2006; A. Torres, 2008; M. Moreno, 2007, 2008, 2010), due its high activation energy and consequently high TCR, and its relatively high room temperature conductivity,  $\sigma_{RT}$ , in comparison with a-Si:H films. In this section is presented a description of the deposition by PECVD of intrinsic amorphous germanium-silicon (a-Ge<sub>x</sub>Si<sub>y</sub>:H) and amorphous germanium-silicon-boron (a-Ge<sub>x</sub>Si<sub>y</sub>B<sub>z</sub>:H) thin films, and its electrical and compositional characterization.

##### 4.1 Films preparation for characterization

An intrinsic film (a-Ge<sub>x</sub>Si<sub>y</sub>:H) was deposited in a capacitive discharge low frequency (LF) PECVD reactor at frequency  $f = 110 \text{ KHz}$ , substrate temperature  $T_s = 300 \text{ }^\circ\text{C}$ , pressure  $P = 0.6$  Torr and RF power  $W = 350 \text{ W}$ , with a gas mixture of SiH<sub>4</sub>, GeH<sub>4</sub> and H<sub>2</sub> and gas flow rates of  $Q_{\text{SiH}_4} = 25 \text{ sccm}$ ,  $Q_{\text{GeH}_4} = 25 \text{ sccm}$  and  $Q_{\text{H}_2} = 1000 \text{ sccm}$  respectively. This result in a Ge gas content  $X_g = 0.5$ . The film was labeled as process A.

The a-Ge<sub>x</sub>Si<sub>y</sub>B<sub>z</sub>:H films were also deposited in a capacitive discharge low frequency (LF) PECVD reactor at frequency  $f = 110 \text{ KHz}$ , substrate temperature  $T_s = 300 \text{ }^\circ\text{C}$ , pressure  $P = 0.6$  Torr and RF power  $W = 350 \text{ W}$ . Three sets of films were deposited from SiH<sub>4</sub> (100%), GeH<sub>4</sub> (100%) and B<sub>2</sub>H<sub>6</sub> (1% on H<sub>2</sub>) gas mixture, with a fixed SiH<sub>4</sub> and B<sub>2</sub>H<sub>6</sub> gas flow rates:  $Q_{\text{SiH}_4} = 50 \text{ sccm}$  and  $Q_{\text{B}_2\text{H}_6} = 500 \text{ sccm}$ , respectively, while the GeH<sub>4</sub> gas flow was set at the following values:  $Q_{\text{GeH}_4} = 25, 50$  and  $75 \text{ sccm}$ .

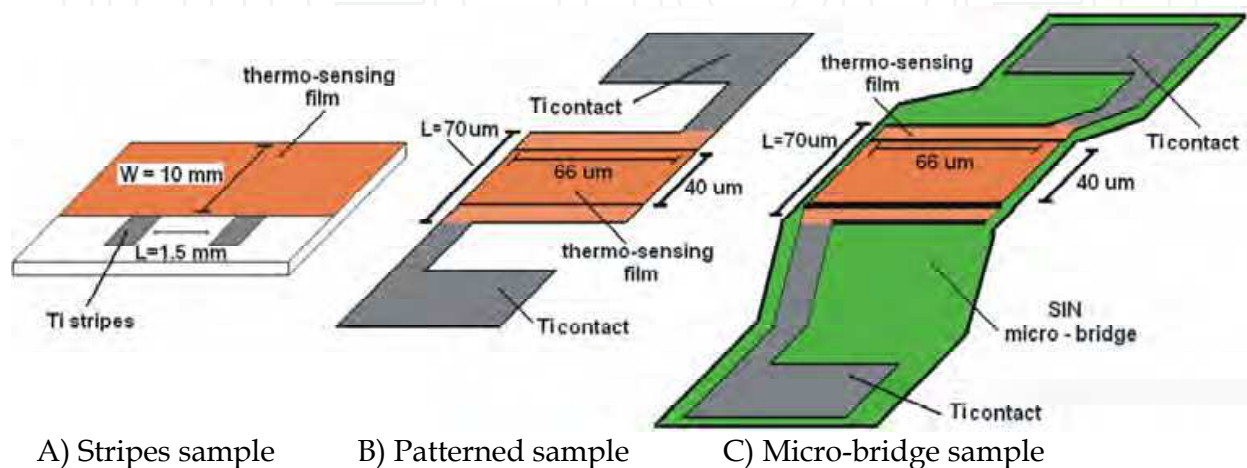
The late resulted in a Ge gas content  $X_g = 0.3, 0.45, 0.55$  and a B gas content  $Z_g = 0.11, 0.09, 0.07$  in the samples labeled as process number B, C and D, respectively. Table 2 shows the deposition parameters for the 4 thermo-sensing films.

	Process A (intrinsic)	Process B	Process C	Process D
Gases flow rates (sccm)	SiH <sub>4</sub> (100%): 25 GeH <sub>4</sub> (100%):25 H <sub>2</sub> : 1000	SiH <sub>4</sub> (100%): 50 GeH <sub>4</sub> (100%): 25 B <sub>2</sub> H <sub>6</sub> (1%): 500	SiH <sub>4</sub> (100%): 50 GeH <sub>4</sub> (100%): 50 B <sub>2</sub> H <sub>6</sub> (1%): 500	SiH <sub>4</sub> (100%): 50 GeH <sub>4</sub> (100%): 75 B <sub>2</sub> H <sub>6</sub> (1%): 500
Dilution ratio (%): $\frac{\text{H}_2}{\text{GeH}_4 + \text{SiH}_4 + \text{B}_2\text{H}_6}$	20	6.2	4.7	3.8
Ge content in gas mixture (%)	50	30	45	55
B content in gas mixture (%)	----	11	9	7
Temperature (°C)	300°C	300°C	300°C	300°C
Pressure (Torr.)	0.6	0.6	0.6	0.6
Frequency (Khz.)	110	110	110	110
Power (W)	300	300	300	300

Table 2. Deposition parameters of a-Ge<sub>x</sub>Si<sub>y</sub>:H and a-Ge<sub>x</sub>Si<sub>y</sub>B<sub>z</sub>:H films.

Since those films are studied for applications as thermo-sensing films for microbolometers, we measured the film electrical properties after patterning them with photolithography in one cell of dimensions  $70 \times 66 \mu\text{m}^2$ .

Assuming that stress arisen in the film deposited over a  $\text{SiN}_x$  micro-bridge could have an effect on the film conductivity, we also studied the films deposited on a micro-bridge. For that purpose, we prepared three different kinds of samples for each type of the four thermo-sensing films (three boron alloys with different Ge content and the intrinsic film). The films were prepared as is shown in Fig. 3.



A) Stripes sample      B) Patterned sample      C) Micro-bridge sample

Fig. 3. Different thermo-sensing films samples. A) Stripes, B) pattern and C) Micro-bridge.

#### 4.2 Temperature dependence of conductivity and TCR in $a\text{-Ge}_x\text{Si}_y\text{:H}$ and $a\text{-Ge}_x\text{Si}_y\text{B}_z\text{:H}$ films

We performed measurements of temperature dependence of conductivity  $\sigma(T)$  in the  $a\text{-Ge}_x\text{Si}_y\text{:H}$  and  $a\text{-Ge}_x\text{Si}_y\text{B}_z\text{:H}$  thermo-sensing films in the range of  $T = 300\text{--}400$  K. The measurements were performed in a vacuum chamber at a pressure  $P \approx 20$  mTorr. A temperature controller (model K-20, MMR Inst.) for the temperature measurement control and an electrometer (model 6517-A, Keithley Inst.) for the current measurements were employed. These measurements allowed us to obtain the  $\sigma(T)$  temperature dependence and then to determine the  $E_a$ , the TCR and the room temperature conductivity,  $\sigma_{RT}$ .

The conductivity temperature dependence can be well described by  $\sigma(T) = \sigma_0 \exp(-E_a/kT)$ , where  $\sigma_0$  is the prefactor,  $E_a$  is the activation energy,  $k$  is the Boltzmann constant and  $T$  is the temperature. Fig. 4 shows  $\sigma(T)$  curves for four different thermo-sensing films (three boron alloys with different Ge gas content,  $\text{Ge}_x = 0.3, 0.45, 0.55$  and the intrinsic film with  $\text{Ge}_x = 0.5$ ), fabricated in three different sample configurations (stripes, patterns and micro-bridges).

From  $\sigma(T)$  measurements with temperature in the thermo-sensing films, we found that the boron alloys ( $a\text{-Ge}_x\text{Si}_y\text{B}_z\text{:H}$ ) have a significantly larger conductivity (by about 2-3 orders of magnitude) in comparison with that of the intrinsic film ( $a\text{-Ge}_x\text{Si}_y\text{:H}$ ). We observed that an increment in the Ge content in gas phase in the boron alloys results in an increase of the room temperature conductivity, from  $\sigma_{RT} = 2.8 \times 10^{-3} (\Omega\text{cm})^{-1}$  (for  $\text{Ge}_x = 0.3$ ) to  $\sigma_{RT} = 1 \times 10^{-2} (\Omega\text{cm})^{-1}$  (for  $\text{Ge}_x = 0.45$ ) and  $\sigma_{RT} = 2.5 \times 10^{-2} (\Omega\text{cm})^{-1}$  (for  $\text{Ge}_x = 0.55$ ), while for the intrinsic film the room temperature conductivity is  $\sigma_{RT} = 6 \times 10^{-5} (\Omega\text{cm})^{-1}$  (for  $\text{Ge}_x = 0.5$ ).

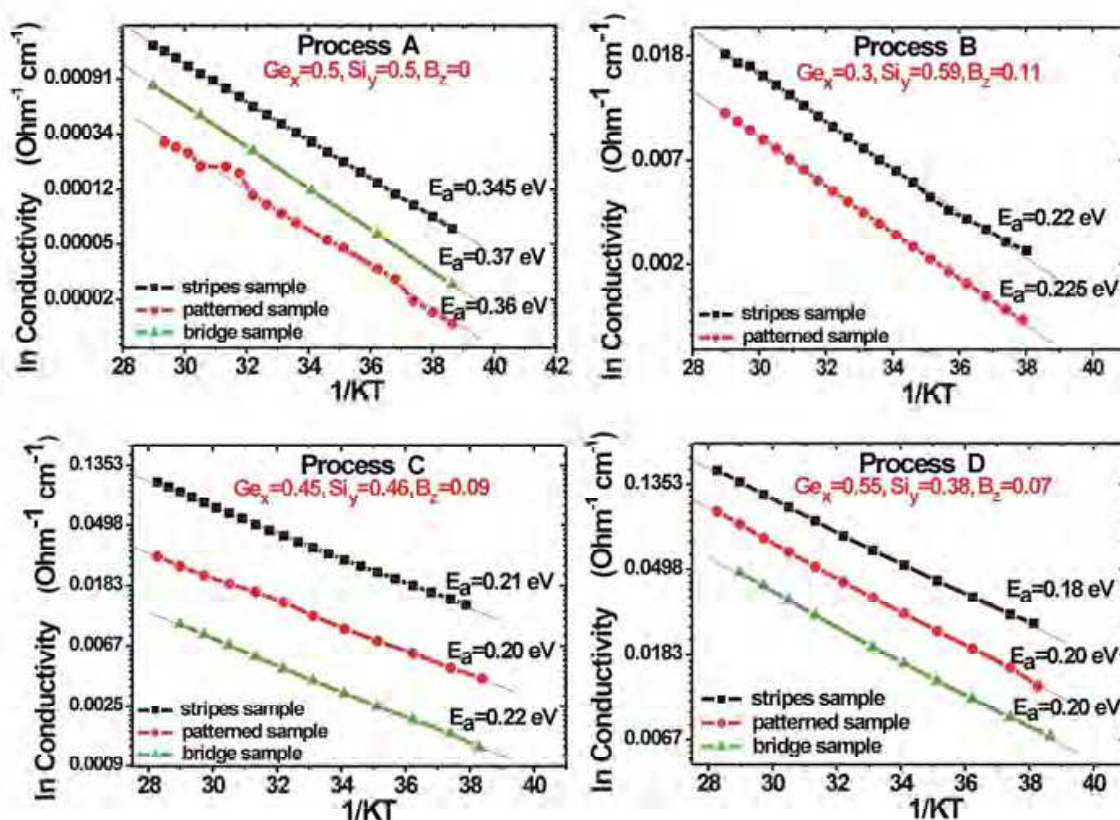


Fig. 4. Conductivity dependence with temperature for the different thermo-sensing films (process: A, B, C and D).

The increment in the  $\sigma$  is accompanied with a reduction in the  $E_a$ . We obtained an  $E_a = 0.22$  eV (for  $\text{Ge}_x = 0.3$ ),  $E_a = 0.21$  eV (for  $\text{Ge}_x = 0.45$ ) and  $E_a = 0.18$  eV (for  $\text{Ge}_x = 0.55$ ), while in the intrinsic film is  $E_a = 0.345$  eV (for  $\text{Ge}_x = 0.5$ ).  $E_a$  as a function of  $\text{Ge}_x$  is shown in Fig. 5 A).

The reduction in the thermo-sensing films dimensions, from the stripes samples ( $10 \times 1.5$  mm<sup>2</sup>) to the patterned samples ( $70 \times 66$   $\mu\text{m}^2$ ), has no significant effect on  $E_a$ , however it has on the  $\sigma_{\text{RT}}$ . We observed a reduction of above 50-80 % of the  $\sigma_{\text{RT}}$  value in the patterned samples in comparison with that of the stripes samples.

Practically no change in  $E_a$  of the thermo-sensing films deposited over a  $\text{SiN}_x$  micro-bridge was observed, in comparison with that of the stripes and patterned samples; however the micro-bridge samples showed a larger reduction in the  $\sigma_{\text{RT}}$  values, of 60-90 %. The dependence of  $\sigma_{\text{RT}}$  with the  $\text{Ge}_x$  content and the sample structure are shown in Fig. 5 B), while the deposition rate dependence of  $\text{Ge}_x$  content in the thermo-sensing films is shown in Fig. 5 C). Table 3 show a comparison of  $E_a$ , TCR,  $\sigma_{\text{RT}}$  and  $\sigma_0$  in stripes, patterned and micro-bridges samples for the different thermo-sensing films.

The micro-bridges samples have the largest reduction of conductivity, and it could be explained by the stress arisen in the  $\text{SiN}_x$  micro-bridge, affecting the thermo-sensing film electrical conductivity. The deposition rate in the boron alloys is around 2 -3 times larger than that of the intrinsic film. Boron incorporation during the thermo-sensing deposition, enhance the deposition rate as is shown in Fig. 5 C).

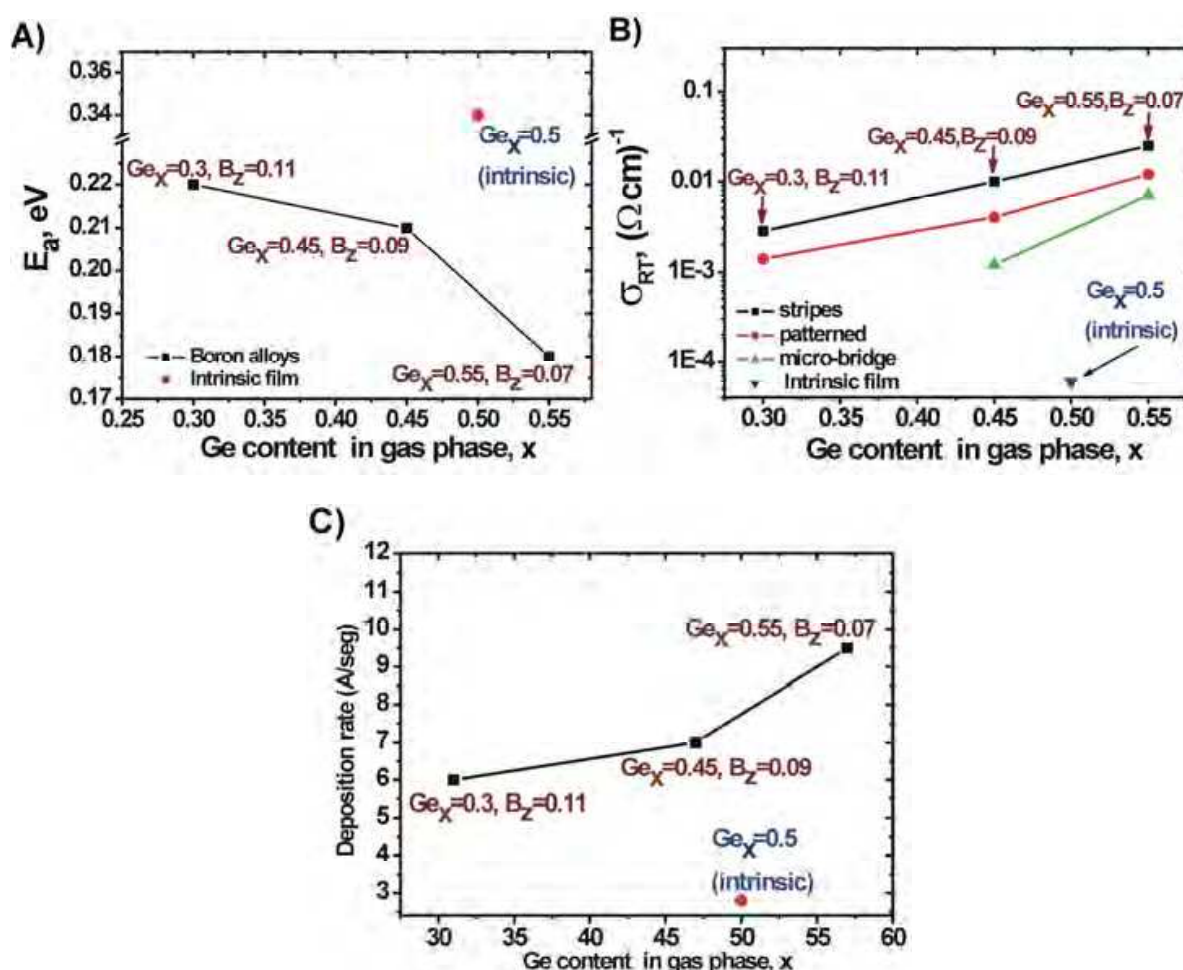


Fig. 5. Characterization of a- $\text{Ge}_x\text{Si}_y\text{:H}$  and a- $\text{Ge}_x\text{Si}_y\text{B}_z\text{:H}$  films. A)  $E_a$  as function of Ge gas content ( $\text{Ge}_x$ ). B) Conductivity as a function of Ge gas content. C) Deposition rate as a function of Ge gas content.

It is important to point out that, doping on amorphous semiconductors reduce  $E_a$  and increases the films conductivity ( $\sigma_{RT}$ ). In Fig 5A) for reference, is shown an intrinsic a- $\text{Ge}_x\text{Si}_y\text{:H}$  film produced with a gas content of  $\text{Ge}_x=50\%$  and  $\text{Si}_y=50\%$ , which has a  $E_a$  of 0.34 eV. This is the largest value for a- $\text{Ge}_x\text{Si}_y\text{:H}$  films (doped or un-doped, using a gas content of  $\text{Ge}_x=50\%$  and  $\text{Si}_y=50\%$ ).

When boron is introduced in the film deposition,  $E_a$  is reduced and the conductivity is increased in the films. In fig. 5 A) is shown that  $E_a$  is reduced to values in the range of 0.18 - 0.22 eV, while the conductivity is increased in more than one order of magnitude. Also it is important to notice that a- $\text{Ge}_x\text{Si}_y\text{:H}$  films have an intermediate  $E_a$  value, between a-Si:H and a-Ge:H. Intrinsic a-Si:H has  $E_a$  values close to 1 eV, while a-Ge:H have  $E_a$  values of above 0.3 eV. Thus, varying the Ge (and Si) gas contents in the a- $\text{Ge}_x\text{Si}_y\text{:H}$  films, it is possible to modify  $E_a$  (an also the conductivity) on intrinsic films.

Larger  $\text{Ge}_x$  content in the films will reduce the value of  $E_a$ . In fig 5 A), we observe a decrement on  $E_a$  of the a- $\text{Ge}_x\text{Si}_y\text{B}_z\text{:H}$  films, not just because the  $B_z$  gas content (which in fact decreases), but because the Ge content (which increases). In fig 5 A) is shown that for a- $\text{Ge}_x\text{Si}_y\text{B}_z\text{:H}$  films, the  $\text{Ge}_x$  gas content vary between 0.3 and 0.55, while the  $B_z$  gas content

vary just between 0.07 and 0.11. Thus the effect of the variation of the Ge gas content on  $E_a$  is dominant in the a-Ge<sub>x</sub>Si<sub>y</sub>B<sub>z</sub>:H films .

### 4.3 Composition of the a-Ge<sub>x</sub>Si<sub>y</sub>:H and a-Ge<sub>x</sub>Si<sub>y</sub>B<sub>z</sub>:H films

In Figure 5 the showed results are related to the Ge<sub>x</sub>, Si<sub>y</sub>, and B<sub>z</sub> gas contents, not to solid contents. There exists a significant difference between the gas content used for the films deposition, and the solid content in the films produced. The composition in solid phase of the different films (three boron alloys with different Ge gas content and the intrinsic film) was characterized by secondary ion mass spectroscopy (SIMS). The samples used for SIMS characterization were the stripes samples described in section 4.1. Fig. 6 shows the SIMS profiles obtained.

From SIMS profiles we calculated the solid composition in the thermo-sensing films. For the film with gas content: Ge<sub>x</sub>=0.3 and B<sub>z</sub>=0.11 (process B), we observed an increase in the solid content: Ge<sub>x</sub>=0.59 and B<sub>z</sub>=0.32 respectively. For the film with Ge<sub>x</sub>=0.45 and B<sub>z</sub>=0.09 (process C), we observed Ge<sub>x</sub>=0.67 and B<sub>z</sub>=0.26, respectively. For the film with Ge<sub>x</sub>=0.55 and B<sub>z</sub>=0.07 (process D), we observed Ge<sub>x</sub>=0.71 and B<sub>z</sub>=0.23, respectively. These results suggested a strong preferential B and Ge incorporation from gas phase during the film deposition process. The B<sub>z</sub> solid content demonstrated values about 3 times larger than the content in gas phase B<sub>z</sub>, while the Ge<sub>x</sub> solid content increased by a factor of 1.3-2 from the Ge<sub>x</sub> gas content. Those results are shown in Table 4.

		Thermo-sensing films			
		Process A	Process B	Process C	Process D
Film Thickness (μm)		0.5	0.36	0.42	0.51
Deposition rate (A/s)		2.8	6	7	9.5
Stripes samples	E <sub>a</sub> (eV)	0.345	0.22	0.21	0.18
	TCR (K <sup>-1</sup> )	-0.044	-0.028	-0.027	-0.023
	σ <sub>RT</sub> (Ωcm) <sup>-1</sup>	6x10 <sup>-5</sup>	2.8x10 <sup>-3</sup>	1x10 <sup>-2</sup>	2.5x10 <sup>-2</sup>
	σ <sub>0</sub> (Ωcm) <sup>-1</sup>	34.85	12.02	36.46	24.55
Patterned samples	E <sub>a</sub> (eV)	0.36	0.225	0.20	0.20
	TCR (K <sup>-1</sup> )	-0.046	-0.029	-0.025	-0.025
	σ <sub>RT</sub> (Ωcm) <sup>-1</sup>	1.08x10 <sup>-5</sup>	1.4x10 <sup>-3</sup>	4x10 <sup>-3</sup>	1.2x10 <sup>-2</sup>
	σ <sub>0</sub> (Ωcm) <sup>-1</sup>	11.13	7.27	8.23	28.26
Micro-bridge samples	E <sub>a</sub> (eV)	0.37	Not available	0.22	0.20
	TCR (K <sup>-1</sup> )	-0.047		-0.028	-0.025
	σ <sub>RT</sub> (Ωcm) <sup>-1</sup>	2.2x10 <sup>-5</sup>		1.2x10 <sup>-3</sup>	7x10 <sup>-3</sup>
	σ <sub>0</sub> (Ωcm) <sup>-1</sup>	32.8		5.94	15.58

Table 3. Comparison of E<sub>a</sub>, TCR, σ<sub>RT</sub> and σ<sub>0</sub> in stripes, patterned and micro-bridges samples for the different thermo-sensing films.

In Fig. 6 the intrinsic film has a Boron content of 10<sup>18</sup> cm<sup>-3</sup> (which represents a B solid content of 2x10<sup>-3</sup> %) as is shown in table 4. The reason of the above is the fact that all the films were deposited on the same chamber. Even though, the chamber was extensively cleaned and coated with a SiN<sub>x</sub> film before the intrinsic film deposition, Boron impurities remained in the chamber walls, which were re-deposited in the intrinsic films.

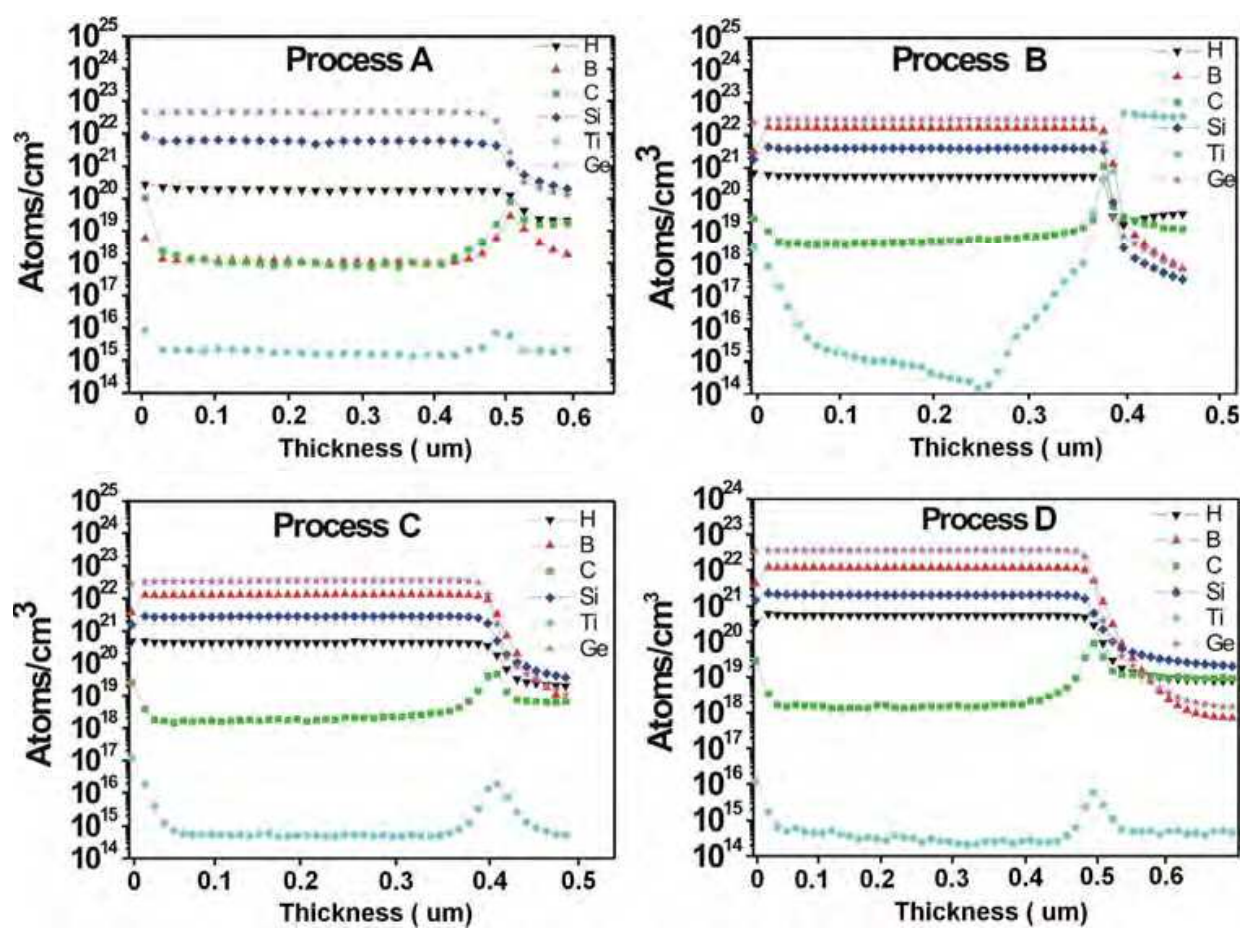


Fig. 6. SIMS profiles of  $a\text{-Ge}_x\text{Si}_y\text{:H}$  and  $a\text{-Ge}_x\text{Si}_y\text{B}_z\text{:H}$  thermo-sensing films.

		Thermo-sensing films			
		Process A	Process B	Process C	Process D
Gas content	$\text{Ge}_x$ (%)	0.5	0.3	0.45	0.55
	$\text{Si}_y$ (%)	0.5	0.59	0.46	0.38
	$\text{B}_z$ (%)	0	0.11	0.09	0.07
Solid content obtained from SIMS	$\text{Ge}_x$ (%)	0.888	0.59	0.67	0.71
	$\text{Si}_y$ (%)	0.110	0.078	0.05	0.04
	$\text{B}_z$ (%)	$2.0 \times 10^{-3}$	0.32	0.26	0.23

Table 4. Gas content and solid content obtained by SIMS for the thermo-sensing films.

## 5. Microbolometer configurations and fabrication process flow

In this section we show a comparative study of the performance characteristics of three configurations of un-cooled microbolometers based on amorphous germanium thin films: a) Planar structure with intrinsic amorphous germanium-silicon  $a\text{-Ge}_x\text{Si}_y\text{:H}$  thermo-sensing film. In this configuration the metal electrodes are placed under the thermo-sensing film (Fig. 7 A); b) Planar structure with amorphous germanium-boron-silicon alloy  $a\text{-Ge}_x\text{B}_y\text{Si}_z\text{:H}$  thermo-sensing film (Fig. 7 B) and c) Sandwich structure with intrinsic  $a\text{-Ge}_x\text{Si}_y\text{:H}$  thermo-sensing film, this configuration consists of metal electrodes which sandwich the thermo-sensing film (Fig. 7 C). Fig. 7 D) shows a picture of one device fabricated.

The fabrication process of the planar structure microbolometer with the  $a\text{-Ge}_x\text{Si}_y\text{:H}$  thermo-sensing film is as follows. A  $0.2\ \mu\text{m}$ -thick  $\text{SiO}_2$  layer is deposited by CVD on a c-Si wafer and a  $2.5\ \mu\text{m}$ -thick sacrificial aluminum layer is deposited by e-beam evaporation and patterned. A  $0.8\ \mu\text{m}$ -thick  $\text{SiN}_x$  film is then deposited at low temperature ( $350\ ^\circ\text{C}$ ) by low frequency PECVD over the aluminum sacrificial film. The  $\text{SiN}_x$  film is patterned by reactive ion etching (RIE) in order to form a  $\text{SiN}_x$  bridge. A  $0.2\ \mu\text{m}$ -thick titanium contacts are deposited by e-beam evaporation over the  $\text{SiN}_x$  bridge and a  $0.5\ \mu\text{m}$ -thick thermo-sensing  $a\text{-Ge}_x\text{Si}_y\text{:H}$  film is deposited over the Ti contacts by low frequency LF PECVD technique at a rf frequency  $f=110\ \text{kHz}$ , temperature  $T=300\ ^\circ\text{C}$ , power  $W=350\ \text{W}$  and pressure  $P=0.6\ \text{Torr}$ . The  $a\text{-Ge}_x\text{Si}_y\text{:H}$  film is deposited from a  $\text{SiH}_4 + \text{GeH}_4 + \text{H}_2$  mixture with gas flows:  $Q_{\text{SiH}_4}=25\ \text{sccm}$ ,  $Q_{\text{GeH}_4}=25\ \text{sccm}$ ,  $Q_{\text{H}_2}=1000\ \text{sccm}$ . This results in a Ge content in solid phase  $Y=0.88$  and a Si content in solid phase  $Y=0.11$ . The thermo-sensing film is covered with a  $0.2\ \mu\text{m}$ -thick absorbing  $\text{SiN}_x$  film deposited by PECVD and finally the aluminum sacrificial layer is removed with wet etching.

The planar structure microbolometer with the boron alloy ( $a\text{-Ge}_x\text{B}_y\text{Si}_z\text{:H}$ ) thermo-sensing film is fabricated as the previous one, with difference in the thermo-sensing film deposition parameters. The boron alloy film is deposited from a  $\text{SiH}_4 + \text{GeH}_4 + \text{B}_2\text{H}_6 + \text{H}_2$  mixture with the following gas flows:  $Q_{\text{SiH}_4}=50\ \text{sccm}$ ,  $Q_{\text{GeH}_4}=50\ \text{sccm}$ ,  $Q_{\text{B}_2\text{H}_6}=5\ \text{sccm}$  and  $Q_{\text{H}_2}=500\ \text{sccm}$ . This results in a Ge content in solid phase  $\text{Ge}_x=0.67$  and B content in solid phase  $\text{B}_y=0.26$ . Those values were obtained by SIMS measurements.

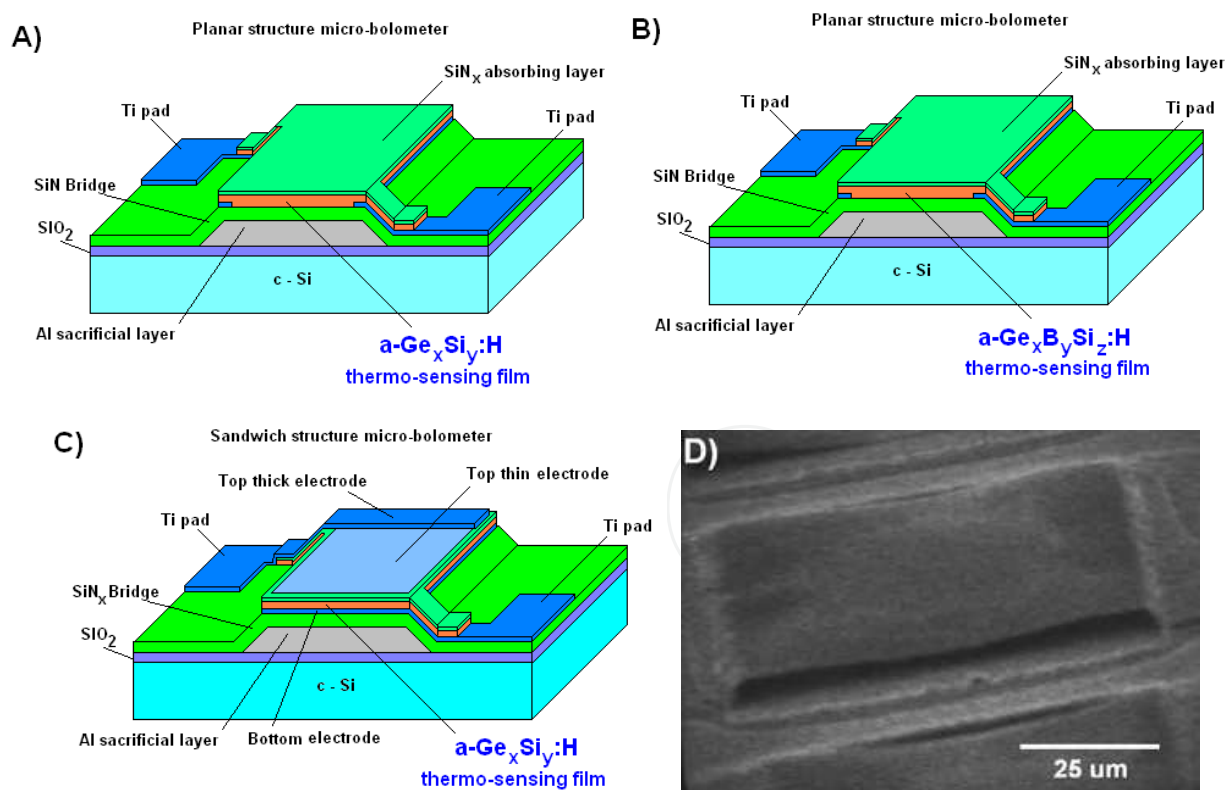


Fig. 7. Microbolometers: A) Planar with intrinsic film  $a\text{-Ge}_x\text{Si}_y\text{:H}$ , B) Planar with boron doped film  $a\text{-Ge}_x\text{B}_y\text{Si}_z\text{:H}$ , C) Sandwich with intrinsic film  $a\text{-Ge}_x\text{Si}_y\text{:H}$ , D) A device fabricated.

The sandwich structure microbolometer with the  $a\text{-Ge}_x\text{Si}_y\text{:H}$  film is fabricated in the same way as the planar microbolometer with some differences, due to the placing of metals as

bottom and top electrodes. In this structure the electrodes sandwich the thermo-sensing film. The bottom Ti electrode is 0.2  $\mu\text{m}$ -thick and is deposited before the thermo-sensing film. Then the  $\text{a-Ge}_x\text{Si}_y\text{:H}$  film is deposited and it is covered with a top thin electrode (10 nm) forming a sandwich structure. The active area of the thermo-sensing layer in the three configurations studied is  $A_b=70 \times 66 \mu\text{m}^2$ . Fig. 8 shows the fabrication process of the microbolometer structures.

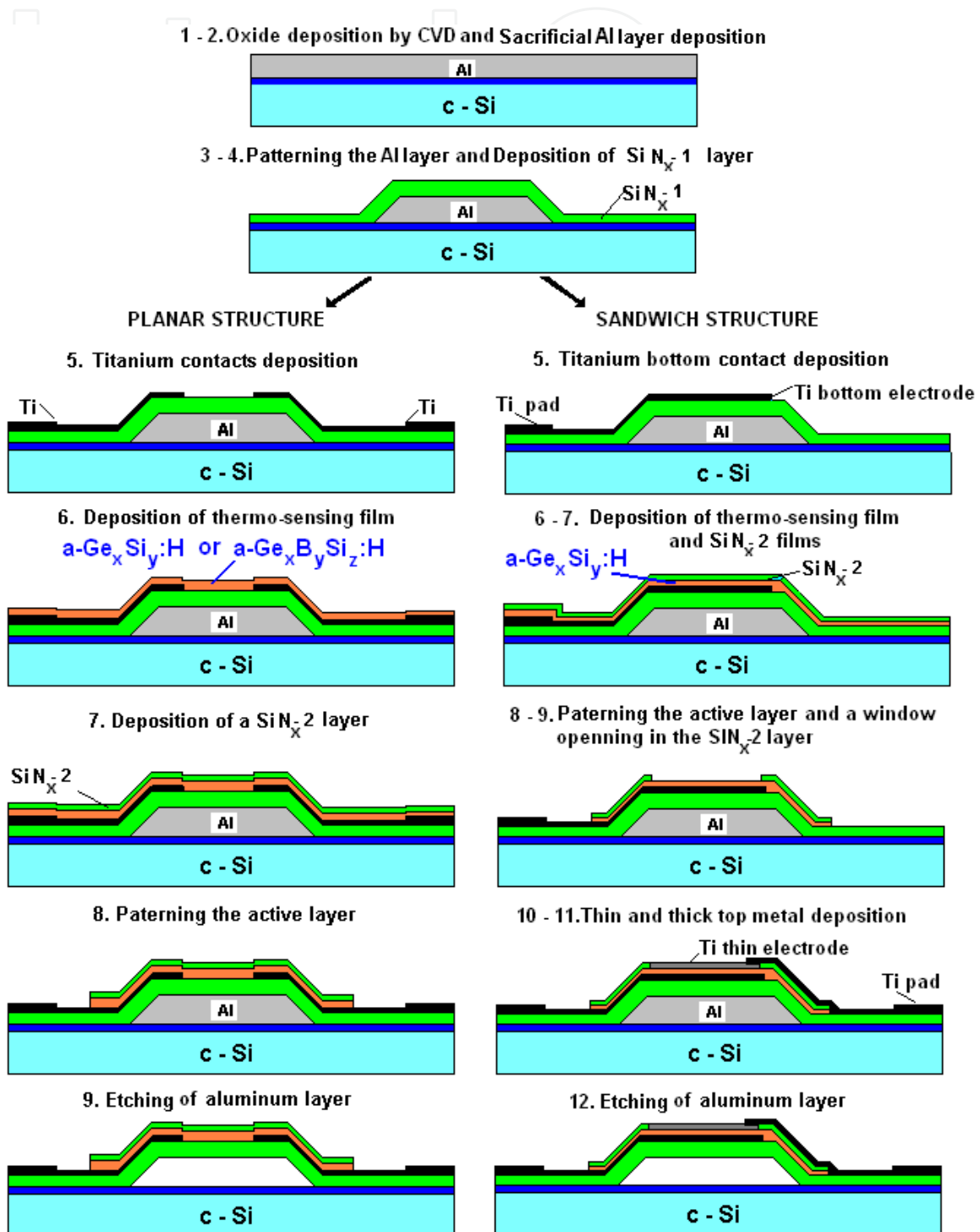


Fig. 8. Planar and sandwich microbolometers fabrication process flow.

## 6. Microbolometers electrical characterization

A microbolometer is a resistor sensitive to temperature change, its operation is based on the temperature increase of the thermo-sensing film by the absorption of the incident IR radiation. The change in temperature causes a change on its electrical resistance, which is measured by an external circuit.

In this section we present a comparative study of 3 configurations of un-cooled microbolometers based on amorphous silicon-germanium thin films deposited by plasma.

### 6.1 I(U) measurements in dark and under Infrared Radiation (IR)

In this section is described the procedure performed in order to obtain the current voltage I(U) characteristics of the microbolometers, from this measurement it is possible to determine the microbolometer electrical resistance and responsivity.

The current-voltage characteristics I(U) and current noise spectral density (NSD) have been measured in the devices in order to compare the performance characteristics, such as responsivity and detectivity in the 3 configurations of microbolometers:

- Planar structure with an intrinsic germanium-silicon (a-Ge<sub>x</sub>Si<sub>y</sub>:H, Ge<sub>x</sub>=0.5) thermo-sensing film (process A of section 4).
- Planar structure with a germanium-silicon-boron alloy (a-Ge<sub>x</sub>Si<sub>y</sub>B<sub>z</sub>:H, Ge<sub>x</sub>=0.45, B<sub>z</sub>=0.09) thermo-sensing film (process C of section 4).
- Sandwich structure with an intrinsic (a-Ge<sub>x</sub>Si<sub>y</sub>:H, Ge<sub>x</sub>=0.5) thermo-sensing film (process A of section 4).

The samples were placed in a vacuum chamber at pressure P≈20 mTorr, at room temperature and illuminated through a zinc selenide window (ZnSe). The window has a 70% transmission in the range of λ=0.6 - 20 μm. The source of IR light is a SiC global source, which provides intensity I<sub>0</sub>=5.3×10<sup>-2</sup> W/cm<sup>2</sup> in the range of λ=1 - 20 μm. The current was measured with an electrometer ("Keithley"- 6517-A) controlled by a PC in dark and under IR illumination.

Fig. 9 A) shows the current-voltage I(U) characteristics in dark and under IR illumination for the planar configuration with a-Ge<sub>x</sub>Si<sub>y</sub>:H thermo-sensing film (process A, section 4); Fig. 9 B) shows these characteristics for the planar configuration with a-Ge<sub>x</sub>Si<sub>y</sub>B<sub>z</sub>:H thermo-sensing film (process C, section 4); and Fig. 9 C) shows the same characteristics for the sandwich configuration with a-Ge<sub>x</sub>Si<sub>y</sub>:H thermo-sensing film (process A, section 4).

In those figures we can see the increment in current due to IR illumination, ΔI=I<sub>IR</sub>-I<sub>Dark</sub>, where I<sub>IR</sub> is the current under IR radiation and I<sub>Dark</sub> is the current in dark. The planar configuration with the a-Ge<sub>x</sub>Si<sub>y</sub>:H (Ge<sub>x</sub>=0.5) film has a ΔI = 5.4 nA (at bias voltage U=7 V); the planar configuration with the a-Ge<sub>x</sub>Si<sub>y</sub>B<sub>z</sub>:H (Ge<sub>x</sub>=0.45, B<sub>z</sub>=0.09) film has a ΔI = 65 nA (at bias voltage U=7 V); and the sandwich configuration with the a-Ge<sub>x</sub>Si<sub>y</sub>:H (Ge<sub>x</sub>=0.5) film has a ΔI = 35 μA (at bias voltage U=4 V). The inset in those figures show the Log I(Log U) characteristics, where we can see their linear behavior. The gamma (γ) constant indicates the slope of the curves.

### 6.2 Current and voltage responsivity

The current responsivity, R<sub>I</sub>, is described by Eq. 17, where ΔI is the increment in current (ΔI=I<sub>IR</sub>-I<sub>Dark</sub>) and P<sub>incident</sub> is the IR incident power in the device surface. P<sub>incident</sub> is described by Eq. 18 and is the product of the cell area, A<sub>cell</sub> and the IR source intensity, I<sub>0</sub>.

$$R_I = \Delta I / P_{\text{incident}} \quad (17)$$

$$P_{\text{incident}} = A_{\text{cell}} I_0 \quad (18)$$

The intensity of the IR source is  $I_0 = 0.053 \text{ Wcm}^{-2}$ , while the cell area is  $A_{\text{cell}} = (70 \times 10^{-4})(66 \times 10^{-4}) \text{ cm}^2 = 4.6 \times 10^{-5} \text{ cm}^2$ . Therefore the IR incident power in the device surface is  $P_{\text{incident}} = 2.475 \times 10^{-6} \text{ W}$ . The planar microbolometer with a- $\text{Ge}_x\text{Si}_y\text{:H}$  ( $\text{Ge}_x=0.5$ ) film has a  $R_I=2 \times 10^{-3} \text{ A/W}$  (at  $U=7 \text{ V}$ ); the planar microbolometer with a- $\text{Ge}_x\text{Si}_y\text{B}_z\text{:H}$  ( $\text{Ge}_x=0.45$ ,  $\text{B}_z=0.09$ ) film has a  $R_I= 3 \times 10^{-2} \text{ A/W}$  (at  $U=7 \text{ V}$ ); and the sandwich microbolometer with a- $\text{Ge}_x\text{Si}_y\text{:H}$  ( $\text{Ge}_x=0.5$ ) film has a  $R_I= 14 \text{ A/W}$  (at  $U=4 \text{ V}$ ).

Table 5 shows the  $\Delta I$  and  $R_I$  values obtained in the configurations. Fig. 10 A) shows the voltage dependence of  $R_I$  for the planar microbolometer with a- $\text{Ge}_x\text{Si}_y\text{:H}$  ( $\text{Ge}_x=0.5$ ) film; Fig. 10 B) shows the voltage dependence of  $R_I$  for the planar microbolometer with a- $\text{Ge}_x\text{Si}_y\text{B}_z\text{:H}$  ( $\text{Ge}_x=0.45$ ,  $\text{B}_z=0.09$ ) film; and Fig. 10 C) shows the voltage dependence of  $R_I$  for the sandwich microbolometer with a- $\text{Ge}_x\text{Si}_y\text{:H}$  ( $\text{Ge}_x=0.5$ ) film. The insert in those figures show a relative current responsivity. Relative current responsivity is the ratio between the increment of current from dark to IR condition,  $\Delta R_I$ , and the microbolometer resistance  $R_{\text{cell}}$ .

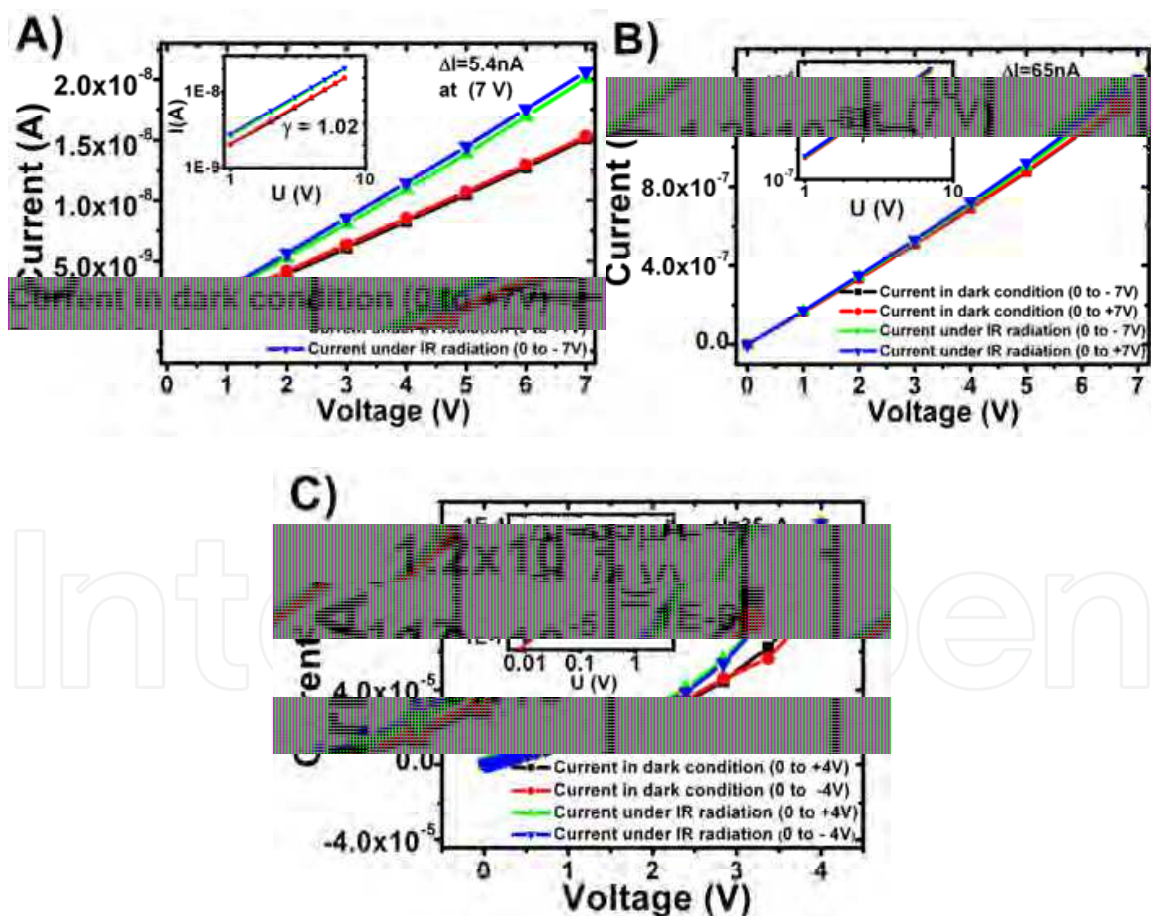


Fig. 9.  $I(U)$  characteristics of 3 microbolometers: A) planar with a- $\text{Ge}_x\text{Si}_y\text{:H}$  ( $\text{Ge}_x=0.5$ ). B) planar with a- $\text{Ge}_x\text{Si}_y\text{B}_z\text{:H}$  ( $\text{Ge}_x=0.45$ ,  $\text{B}_z=0.09$ ). C) sandwich with a- $\text{Ge}_x\text{Si}_y\text{:H}$  ( $\text{Ge}_x=0.5$ ). The inset in those figures show the Log I(Log U) characteristics, where we can see their linear behavior. The gamma ( $\gamma$ ) constant indicates the slope of the curves.

The planar and sandwich structures with the intrinsic film show larger values of relative current responsivity. The voltage responsivity,  $R_U$ , was calculated from the experimental  $I(U)$  points, the increment in voltage from dark condition to IR condition was obtained from a fixed current. Fig. 11 A) shows a  $\Delta U = 1.8$  V extracted from a fixed current  $I = 1.5 \times 10^{-8}$  A, in the planar structure microbolometer with the a-Ge<sub>x</sub>Si<sub>y</sub>:H ( $Ge_x=0.5$ ) film. Fig. 11 B) shows a  $\Delta U = 0.3$  V extracted from a fixed current  $I = 1.35 \times 10^{-6}$  A, in the planar structure microbolometer with the a-Ge<sub>x</sub>Si<sub>y</sub>B<sub>z</sub>:H ( $Ge_x=0.45, B_z=0.09$ ) film. Fig. 11 C) shows a  $\Delta U = 0.54$  V extracted from a fixed current  $I = 1.16 \times 10^{-4}$  A, in the sandwich structure microbolometer with the a-Ge<sub>x</sub>Si<sub>y</sub>:H ( $Ge_x=0.5$ ) film.

	Planar structure With a-Ge <sub>x</sub> Si <sub>y</sub> :H	Planar structure With a-Ge <sub>x</sub> Si <sub>y</sub> B <sub>z</sub> :H	Sandwich structure With a-Ge <sub>x</sub> Si <sub>y</sub> :H
Film process	A	C	A
$\Delta I = I_{IR} - I_{dark}$ (A)	$5.4 \times 10^{-9}$ (at $U=7$ V)	$65 \times 10^{-9}$ (at $U=7$ V)	$35 \times 10^{-6}$ (at $U=4$ V)
Current responsivity ( $AW^{-1}$ )	$2 \times 10^{-3}$	$3 \times 10^{-2}$	14
$\Delta U = U_{IR} - U_{dark}$ (V)	1.8 (at $I=1.5 \times 10^{-8}$ )	0.3 (at $I=1.35 \times 10^{-6}$ )	0.54 (at $I=1.16 \times 10^{-4}$ )
Voltage Responsivity ( $VW^{-1}$ )	$7.2 \times 10^5$	$1.2 \times 10^5$	$2.2 \times 10^5$

Table 5. Current and voltage responsivity values for 3 microbolometer configurations.

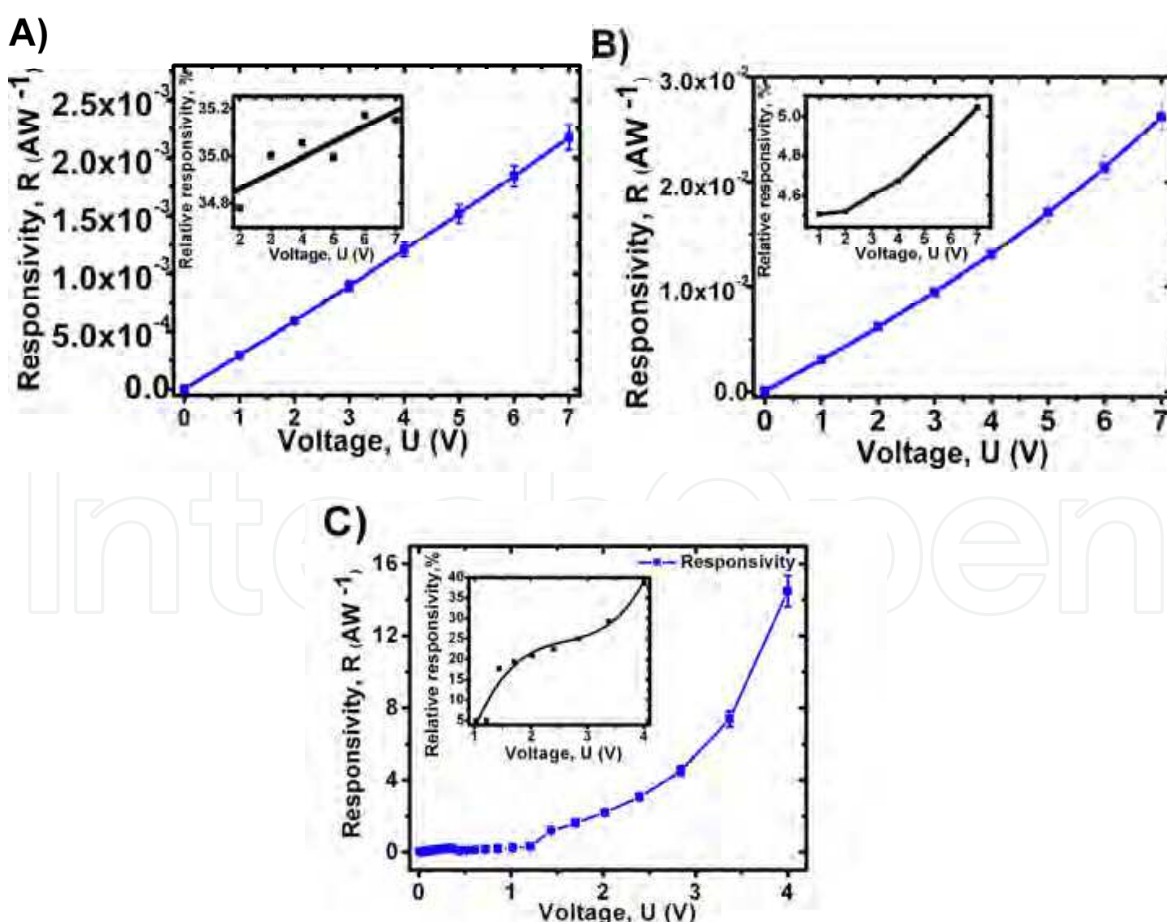


Fig. 10. Voltage dependence of  $R_I$  of 3 microbolometers: A) planar with a-Ge<sub>x</sub>Si<sub>y</sub>:H ( $Ge_x=0.5$ ). B) planar with a-Ge<sub>x</sub>Si<sub>y</sub>B<sub>z</sub>:H ( $Ge_x=0.45, B_z=0.09$ ). C) sandwich with a-Ge<sub>x</sub>Si<sub>y</sub>:H ( $Ge_x=0.5$ ).

The planar microbolometer with a-Ge<sub>x</sub>Si<sub>y</sub>:H (Ge<sub>x</sub>=0.5) film has a  $R_U=7.2 \times 10^5$  V/W (at  $I=1.5 \times 10^{-8}$  A); the planar microbolometer with a-Ge<sub>x</sub>Si<sub>y</sub>B<sub>z</sub>:H (Ge<sub>x</sub>=0.45, B<sub>z</sub>=0.09) film has a  $R_U=1.2 \times 10^5$  V/W (at  $I=1.4 \times 10^{-6}$  A); and the sandwich microbolometer with a-Ge<sub>x</sub>Si<sub>y</sub>:H (Ge<sub>x</sub>=0.5) film has a  $R_U=2.2 \times 10^5$  V/W (at  $I=1.16 \times 10^{-4}$  A). Table 5 shows the  $\Delta U$  and  $R_U$  values obtained from the different microbolometers configurations.

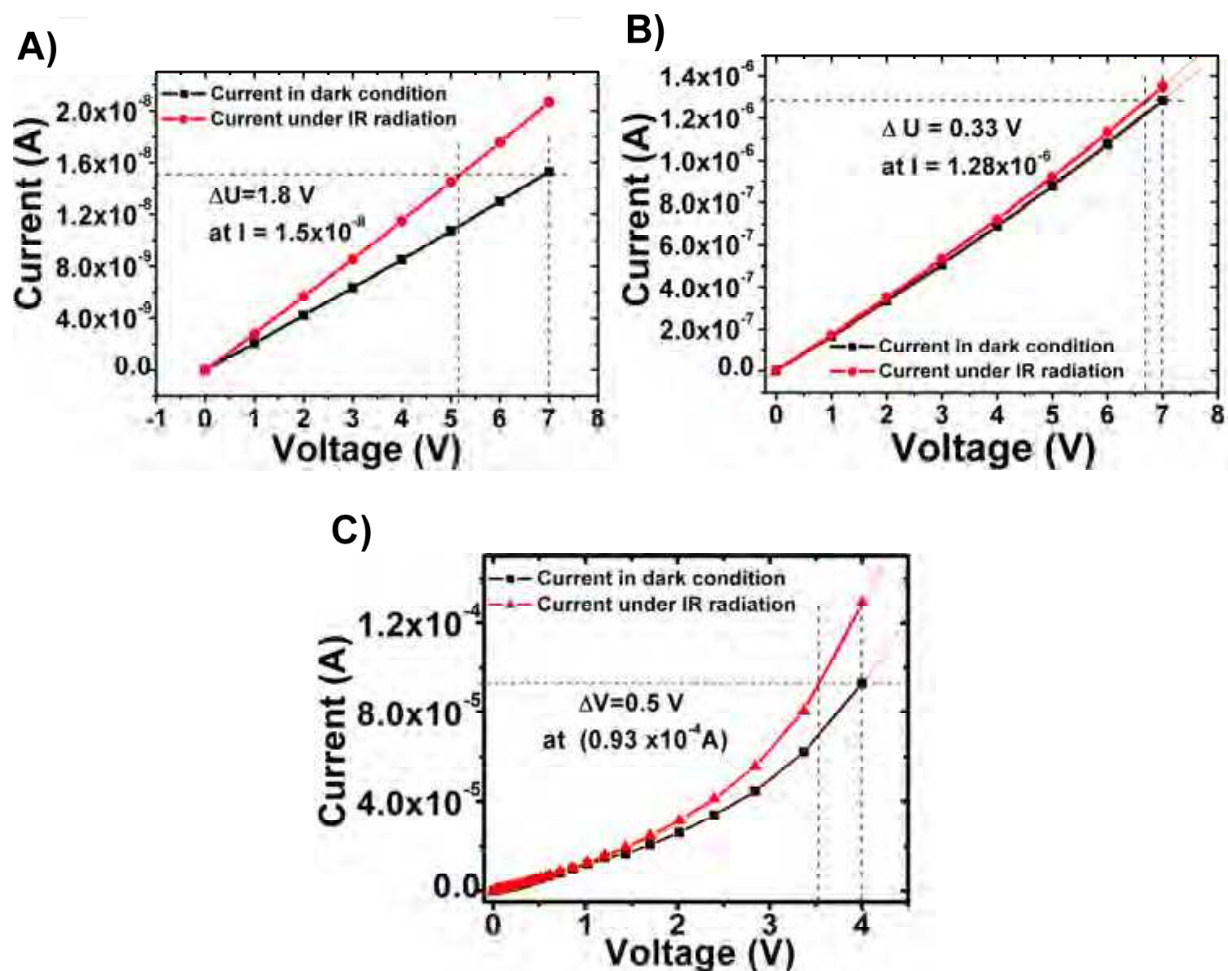


Fig. 11. Extraction of  $\Delta U$  from  $I(U)$  characteristics: A) planar with a-Ge<sub>x</sub>Si<sub>y</sub>:H (Ge<sub>x</sub>=0.5). B) planar with a-Ge<sub>x</sub>Si<sub>y</sub>B<sub>z</sub>:H (Ge<sub>x</sub>=0.45, B<sub>z</sub>=0.09). C) sandwich with a-Ge<sub>x</sub>Si<sub>y</sub>:H (Ge<sub>x</sub>=0.5).

### 6.3 Noise spectral density measurements and detectivity calculations

Noise measurements in the microbolometers were performed with a lock-in amplifier ("Stanford Research Systems" - SR530). The noise of the system and the total noise (system + cell noise) were measured separately, and a subtraction of the system noise allowed us to obtain the noise of the device. The detectivity was calculated from the responsivity values and noise measurements. The current noise spectral density (NSD),  $I_{\text{cell noise}}(f)$ , of the fabricated devices with the different thermo-sensing films are shown in Fig. 12.

The NSD in the cell is obtained as  $(I_{\text{cell noise}}(f))^2 = (I_{\text{system + cell noise}}(f))^2 - (I_{\text{system noise}}(f))^2$ , where  $I_{\text{cell + system noise}}(f)$  is the NSD measured at the microbolometer with the measuring system and the  $I_{\text{system noise}}(f)$  is the NSD measured in the system without the microbolometer. In noise

curves we observed different slopes at different frequencies and different cone frequencies. That data are shown in Table 6, where  $f_{c1}$  is the cone frequency 1,  $f_{c2}$  is the cone frequency 2,  $\beta$  is the slope of the curve in region 1 and  $\gamma$  is the slope of the curve in region 2.

The planar structure with a-Ge<sub>x</sub>Si<sub>y</sub>:H (Ge<sub>x</sub>=0.5) film shows  $I_{\text{cell noise}}(f) \approx 10^{-16} \text{ AHz}^{-1/2}$ ; the planar structure with a-Ge<sub>x</sub>Si<sub>y</sub>B<sub>z</sub>:H (Ge<sub>x</sub>=0.45, B<sub>z</sub>=0.09) film shows  $I_{\text{cell noise}}(f) \approx 10^{-14} \text{ AHz}^{-1/2}$ ; and the sandwich structure with a-Ge<sub>x</sub>Si<sub>y</sub>:H (Ge<sub>x</sub>=0.5) has  $I_{\text{cell noise}}(f) \approx 10^{-11} \text{ AHz}^{-1/2}$ .

The procedure for the detectivity calculation is shown in Eq. 19, where  $R_I$  is the current responsivity,  $A_{\text{cell}}$  is the detector area,  $I_{\text{noise}}$  is the cell NSD and  $\Delta f = 1$  is the bandwidth of the measurement system.

$$D^* = R_I (A_{\text{cell}})^{1/2} / I_{\text{noise}} / (\Delta f)^{1/2} \quad (19)$$

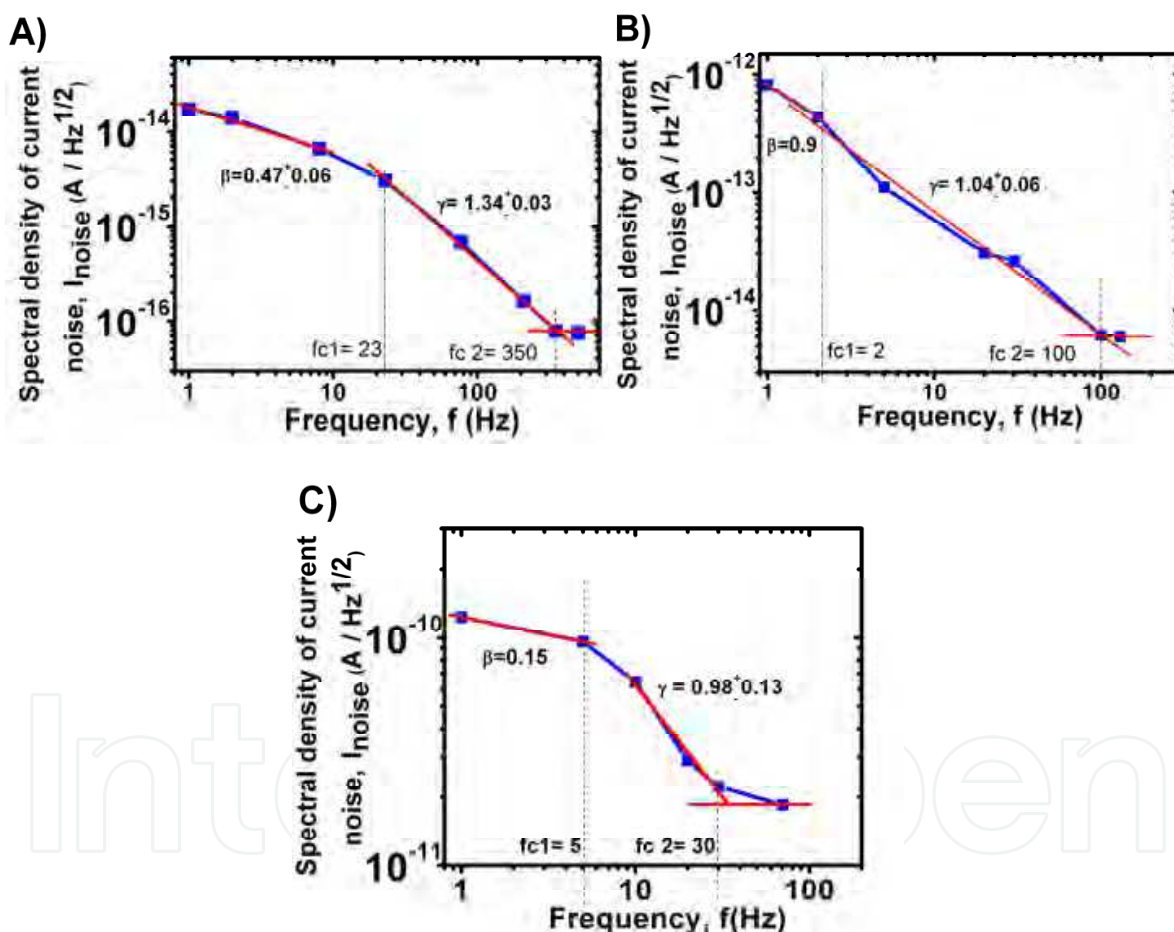


Fig. 12. Spectral density of current noise (NSD) of 3 microbolometers: A) planar with a-Ge<sub>x</sub>Si<sub>y</sub>:H (Ge<sub>x</sub>=0.5). B) planar with a-Ge<sub>x</sub>Si<sub>y</sub>B<sub>z</sub>:H (Ge<sub>x</sub>=0.45, B<sub>z</sub>=0.09). C) sandwich with a-Ge<sub>x</sub>Si<sub>y</sub>:H (Ge<sub>x</sub>=0.5).

We calculated the detectivity values  $D^*$  in the 3 structures. For the planar structure with the a-Ge<sub>x</sub>Si<sub>y</sub>:H (Ge<sub>x</sub>=0.5) film we obtained  $D^* = 7 \times 10^9 \text{ cmHz}^{1/2}\text{W}^{-1}$ ; for the planar structure with the a-Ge<sub>x</sub>Si<sub>y</sub>B<sub>z</sub>:H (Ge<sub>x</sub>=0.45, B<sub>z</sub>=0.09) film it is  $D^* = 5.9 \times 10^9 \text{ cmHz}^{1/2}\text{W}^{-1}$ ; and for the sandwich structure microbolometer with the a-Ge<sub>x</sub>Si<sub>y</sub>:H (Ge<sub>x</sub>=0.5) film it is  $D^* = 4 \times 10^9 \text{ cmHz}^{1/2}\text{W}^{-1}$ .

Samples	Frequency Regions				
	Region no. 1		Region no. 2		Region no. 3
	$\beta$	fc1 (Hz.)	$\gamma$	fc2 (Hz.)	Noise level (AHz <sup>-1/2</sup> )
Planar structure a-Ge <sub>x</sub> Si <sub>y</sub> :H (Ge <sub>x</sub> =0.5)	0.47	23	1.34	350	10 <sup>-16</sup>
Planar structure a-Ge <sub>x</sub> Si <sub>y</sub> B <sub>z</sub> :H (Ge <sub>x</sub> =0.45, B <sub>z</sub> =0.09)	0.9	2	1.04	100	10 <sup>-14</sup>
Sandwich structure a-Ge <sub>x</sub> Si <sub>y</sub> :H (Ge <sub>x</sub> =0.5)	0.15	5	0.98	30	10 <sup>-11</sup>

Table 6. NSD at different frequency regions in the different microbolometers structures.

## 7. Microbolometers thermal characterization and calibration curve

In order to estimate the temperature dependence of the thermal resistance of the microbolometers,  $I(U)$  measurements were performed in the range from 260 K to 360 K, as is shown in Fig. 13 A), where the bias is plotted as a function of current.

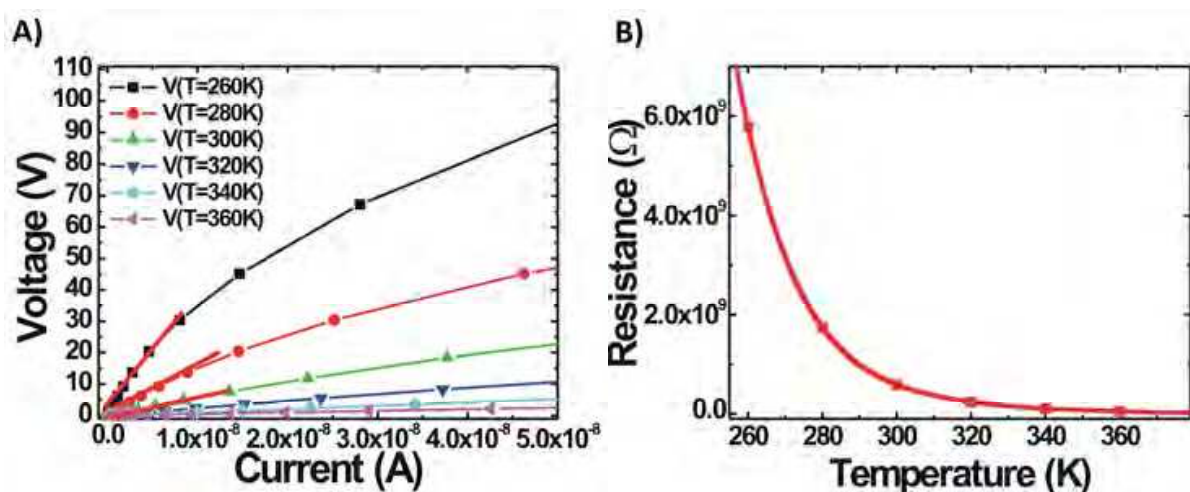


Fig. 13. A)  $U(I)$  curves of a planar structure microbolometer with a-Ge<sub>x</sub>Si<sub>y</sub>:H (Ge<sub>x</sub>=0.5). B) Calibration curve of a planar structure microbolometer with a-Ge<sub>x</sub>Si<sub>y</sub>:H (Ge<sub>x</sub>=0.5).

The slope of the linear part of each curve showed in Fig. 13 A) corresponds to the electrical resistance of the microbolometer for each temperature value (in the range of 260 K - 360 K). Once that is obtained the value of the electrical resistance for each value of temperature, it is possible to graph the electrical resistance of the microbolometer as a function of the temperature, also called the calibration curve, as is shown in Fig. 13 B).

The calibration curve is very important because from this curve is possible to calculate an increment in temperature in the microbolometer by measuring a change in its resistance.

The voltage-current curves in Fig. 13 A) have different resistance values as the current increases. The value of the resistance is affected by the temperature. Thus the resistance is calculated for each point of the Voltage-Current curves (obtained at different temperatures, 260, 270, etc.). If the resistance values obtained are compared with the calibration curve, it is possible to extract the increment of temperature ( $\Delta T$ ) for each point.

Fig. 14 A) shows the increment of temperature ( $\Delta T$ ) as a function of the power ( $P=U*I$ ) applied to the microbolometer, for each temperature.

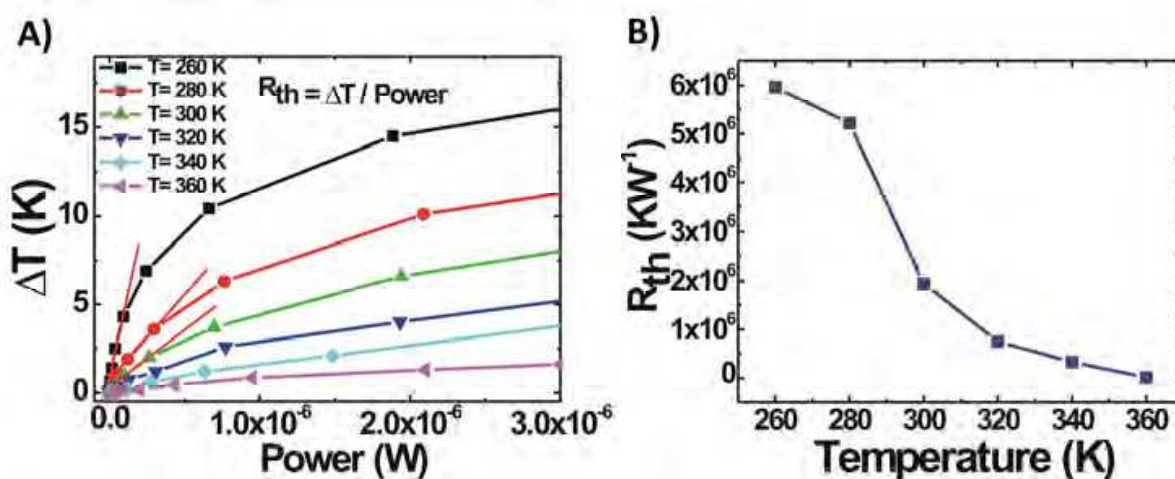


Fig. 14. A)  $\Delta T$  vs Power curve of a microbolometer. B) Thermal resistance of a planar structure microbolometer with  $a\text{-Ge}_x\text{Si}_y\text{:H}$  ( $\text{Ge}_x=0.5$ ).

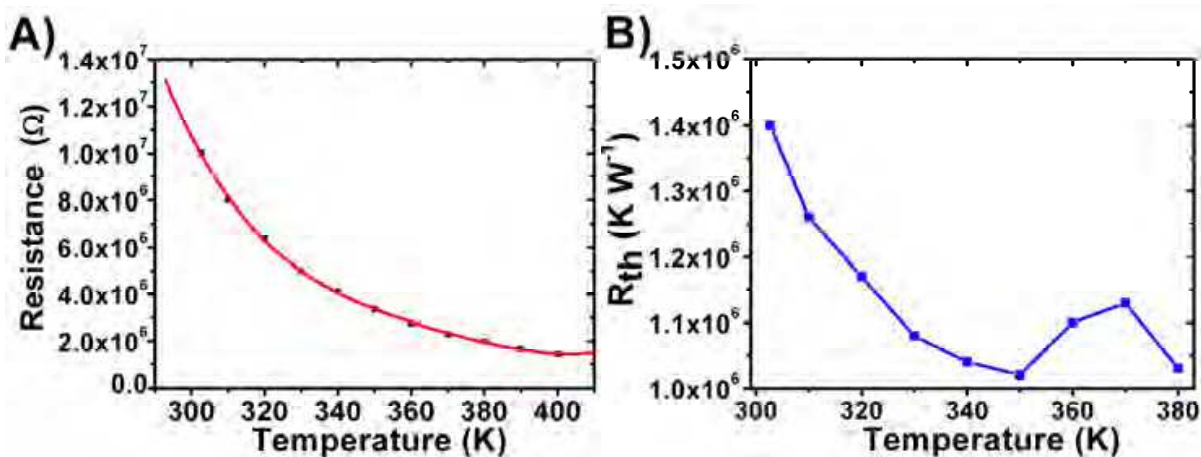


Fig. 15. Microbolometer with  $a\text{-Ge}_x\text{Si}_y\text{B}_z\text{:H}$  ( $\text{Ge}_x=0.45$ ,  $\text{B}_z=0.09$ ). A) Calibration curve. B) Thermal resistance.

The thermal resistance of the microbolometer,  $R_{th}$ , is then obtained as the slope of the increment of temperature in the microbolometer ( $\Delta T$ ) as a function of the power applied to it, for each temperature value. Fig. 14 B) shows the temperature dependence of the thermal resistance ( $R_{th}$ ). Fig. 15 A) shows the calibration curve and Fig. 15 B) shows the temperature dependence of the thermal resistance ( $R_{th}$ ) of the planar structure microbolometer with  $a\text{-Ge}_x\text{Si}_y\text{B}_z\text{:H}$  ( $\text{Ge}_x=0.45$ ,  $\text{B}_z=0.09$ ).

### 8. $a\text{-Ge}_x\text{Si}_y\text{:H}$ and $a\text{-Ge}_x\text{Si}_y\text{B}_z\text{:H}$ microbolometers compared with literature

The results obtained from the study of fabrication and characterization of different microbolometer structures, containing intrinsic  $a\text{-Ge}_x\text{Si}_y\text{:H}$  films and boron alloys  $a\text{-Ge}_x\text{Si}_y\text{B}_z\text{:H}$ , are discussed in the present section and compared with data reported in literature.

### 8.1 Thermo-sensing film characterization

Table 7 shows the most employed materials as thermo-sensing films in microbolometers.  $\text{VO}_x$  is one of the most employed materials (B. E. Cole, 1998), however this material is not compatible with Si CMOS standard technology and its TCR is not very large, around  $0.021 \text{ K}^{-1}$ . Amorphous  $\text{Ge}_x\text{Si}_{1-x}\text{O}_y$  films have been employed in microbolometers (E. Iborra, 2002), these films are compatible with the CMOS technology and present a high TCR, around  $0.042 \text{ K}^{-1}$ ; however also have a high resistance.

Material	TCR ( $\text{K}^{-1}$ )	Ea (eV)	$\sigma_{\text{RT}}$ ( $\Omega \text{ cm}$ ) <sup>-1</sup>	Reference
$\text{VO}_x$	0.021	0.16	$2 \times 10^{-1}$	B. E. Cole, 1998
a-Si:H (PECVD)	0.1 - 0.13	0.08-1	$\sim 1 \times 10^{-9}$	A. J. Syllaios, 2000
a-Si:H,B (PECVD)	0.028	0.22	$5 \times 10^{-3}$	A. J. Syllaios, 2000
a- $\text{Ge}_x\text{Si}_y\text{:H}$ (PECVD)*	0.043	0.34	$1.6 \times 10^{-6}$	M. Moreno, 2008
$\text{Ge}_x\text{Si}_{1-x}\text{O}_y$	0.042	0.32	$2.6 \times 10^{-2}$	E. Iborra, 2002

Table 7. Most common thermo-sensing materials employed in microbolometers.

At the present time a-Si:H and boron doped a-Si:H are employed in large microbolometer arrays (A. J. Syllaios, 2000). Intrinsic a-Si:H is compatible with CMOS technology and has a very high TCR, around  $0.1-0.13 \text{ K}^{-1}$ ; however it is a highly resistive material, resulting in high resistive microbolometers which present a mismatch impedance with the readout circuits. Boron doped a-Si:H, has moderated resistivity, but also a reduced TCR, of  $0.028 \text{ K}^{-1}$ . Therefore none of those materials can be considered the optimum one as thermo-sensing material in microbolometers. Intrinsic a- $\text{Ge}_x\text{Si}_y\text{:H}$  films presents a large TCR, around  $0.043 \text{ K}^{-1}$ , a moderated resistivity and is compatible with the Si CMOS technology; those characteristics make this material suitable as thermo-sensing film for microbolometer arrays, however the resistivity is still an issue.

Amorphous germanium-silicon-boron alloys a- $\text{Ge}_x\text{Si}_y\text{B}_z\text{:H}$ , have been studied in order to reduce the high resistivity presented in intrinsic films. From the conductivity characterization in the thermo-sensing films, we can state that the a- $\text{Ge}_x\text{Si}_y\text{B}_z\text{:H}$  alloys demonstrated an increment in their conductivity (between 2 and 3 orders of magnitude) in comparison with that of the intrinsic a- $\text{Ge}_x\text{Si}_y\text{:H}$  film. However the increment in  $\sigma_{\text{RT}}$  was accompanied by a reduction in TCR, to above  $0.028 \text{ K}^{-1}$ .

The deposition rate in the boron alloys is above 2-3 times larger than that of the intrinsic film. Thus B incorporation during the thermo-sensing deposition, enhance the deposition rate. The deposition of the thermo-sensing films over a  $\text{SiN}_x$  micro-bridge, has as consequence a reduction in the film conductivity, the stress arisen in the  $\text{SiN}_x$  micro-bridge could be the cause for the  $\sigma_{\text{RT}}$  reduction. The a- $\text{Ge}_x\text{Si}_y\text{B}_z\text{:H}$  films compared with the another thermo-sensing materials, have better performance characteristics, which are: compatibility with the Si CMOS technology, moderated values of TCR, comparables with those of the  $\text{VO}_x$  and a-Si:H films, and reduced resistivity. In general the a- $\text{Ge}_x\text{Si}_y\text{B}_z\text{:H}$  alloys have similar characteristics than those of the a-Si:H,B thermo-sensing film (A. J. Syllaios, 2000), but also have one order of magnitude shorter resistivity.

### 8.2 Microbolometers characterization

Table 8 shows the main performance characteristics of the microbolometers reported in literature, which are compared with the different microbolometer configurations studied in

this work, containing intrinsic and boron alloys thermo-sensing films. Commercial planar structure microbolometers based on VO<sub>x</sub> films (B. E. Cole, 1998), present moderated values of TCR, around  $\alpha=0.021$  K<sup>-1</sup> and high values of voltage responsivity,  $R_U=2.5 \times 10^7$  VW<sup>-1</sup>. Another performance characteristics as detectivity,  $D^*$  are not published. The main drawback of these devices is their un-compatibility with Si CMOS technology, thus special installations are necessary for their fabrication, which make impossible to fabricate those devices in any standard Si CMOS fabrication line.

Thermo sensing film	E <sub>a</sub> , eV	TCR, $\alpha$ K <sup>-1</sup>	Cell area, A <sub>cell</sub> , $\mu\text{m}^2$	Cell resistance, R <sub>cell</sub> , Ohm	Voltage responsivity R <sub>U</sub> , VW <sup>-1</sup>	Currentes ponsivity, R <sub>I</sub> , AW <sup>-1</sup>	Detectivity, D <sup>*</sup> , cmHz <sup>1/2</sup> W <sup>-1</sup>	References
VO <sub>x</sub>	0.16	0.021	50 x 50	-	$2.5 \times 10^7$	-	-	B. E. Cole, 1998
Ge <sub>x</sub> Si <sub>1-x</sub> O <sub>y</sub>	0.32	0.042	50 x 50	$7 \times 10^5$	$1 \times 10^5$	-	$6.7 \times 10^8$	E. Iborra, 2002
a-Si:H,B	0.22	0.028	48 x 48	$3 \times 10^7$	$10^6$	-	-	A. J. Syllaios, 2000
a-Si:H	0.8-1	0.039	25 x 25	$>10^9$	-	-	-	A. J. Syllaios, 2000
a-Ge <sub>x</sub> Si <sub>y</sub> :H Ge <sub>x</sub> =0.5	0.34	0.043	70 x 66	$5 \times 10^8$	$7.2 \times 10^5$ *	$2 \times 10^{-3}$	$7.9 \times 10^9$	Planar M. Moreno, 2008
a-Ge <sub>x</sub> Si <sub>y</sub> B <sub>z</sub> :H Ge <sub>x</sub> =0.45, B <sub>z</sub> =0.09	0.21	0.027	70 x 66	$1 \times 10^6$	$1.2 \times 10^5$ *	$3 \times 10^{-2}$	$5.9 \times 10^9$	Planar M. Moreno, 2008
a-Ge <sub>x</sub> Si <sub>y</sub> B <sub>z</sub> :H Ge <sub>x</sub> =0.55, B <sub>z</sub> =0.07	0.20	0.028	70 x 66	$3 \times 10^6$	$1.8 \times 10^5$ *	$7 \times 10^{-2}$	$2 \times 10^9$	Planar M. Moreno, 2008
a-Ge <sub>x</sub> Si <sub>y</sub> :H Ge <sub>x</sub> =0.5	0.34	0.043	70 x 66	$1 \times 10^5$	$2.2 \times 10^5$ *	0.3 - 14	$4 \times 10^9$	Sandwich M. Moreno, 2008

Table 8. Comparison of characteristics of micro-bolometers with literature.

Planar structure microbolometers based on resistive a-Si:H, present high values of TCR, around  $\alpha=0.1-0.13$  K<sup>-1</sup>, however also have very high values of resistance. Comercial a-Si:H,B based planar structure microbolometers (A. J. Syllaios, 2000) have moderated values of TCR, around  $\alpha=0.28$  K<sup>-1</sup>, a cell resistance  $R_{\text{cell}} = 3 \times 10^7$   $\Omega$ , and a high voltage responsivity, around  $R_U = 10^6$  VW<sup>-1</sup>. However values of  $D^*$  are not reported.

Microbolometers based on a-Ge<sub>x</sub>Si<sub>1-x</sub>O<sub>y</sub> (E. Iborra, 2002) have demonstrated high values of TCR, around  $\alpha=0.042$  K<sup>-1</sup>, a moderated cell resistance,  $R_{\text{cell}} = 7 \times 10^5$   $\Omega$ , and moderated detectivity  $D^*=6.7 \times 10^8$  cmHz<sup>1/2</sup>W<sup>-1</sup>.

In our work, the planar structure microbolometers based on intrinsic a-Ge<sub>x</sub>Si<sub>y</sub>:H films have a very high value of TCR, around  $\alpha=0.043$  K<sup>-1</sup>, a current responsivity,  $R_I=2 \times 10^{-3}$  AW<sup>-1</sup>, a very

low current NSD,  $I_{\text{noise}} \approx 1 \times 10^{-15} \text{ AHz}^{-1/2}$ , resulting in a very high detectivity  $D^* = 7.9 \times 10^9 \text{ cmHz}^{1/2}\text{W}^{-1}$ . However those devices still have a high cell resistance,  $R_{\text{cell}} = 5 \times 10^8 \Omega$ .

The boron alloy planar structure microbolometers have a cell resistance, around  $R_{\text{cell}} \approx (1-3) \times 10^6 \Omega$ , which is two orders of magnitude shorter than that of the planar structure devices with intrinsic film and one order of magnitude shorter than that of the a-Si:H,B commercial devices (A. J. Syllaios, 2000). The current responsivity is around  $R_I = (3-7) \times 10^{-2} \text{ AW}^{-1}$ , and the current NSD,  $I_{\text{noise}} \approx 10^{-13} \text{ AHz}^{-1/2}$ , which results in a high detectivity  $D^* = (2-6) \times 10^9 \text{ cmHz}^{1/2}\text{W}^{-1}$ .

The sandwich structure microbolometer with the intrinsic a- $\text{Ge}_x\text{Si}_y\text{:H}$  film, presents the shortest cell resistance of the devices reported in literature,  $R_{\text{cell}} \approx 1 \times 10^5 \Omega$ , which is 3 orders of magnitude less than that of the planar devices with the same intrinsic film; one order of magnitude shorter than that of the boron alloy devices; 2 orders shorter than that of the a-Si:H,B devices; and near to 1 order of magnitude shorter than that of the a- $\text{Ge}_x\text{Si}_{1-x}\text{O}_y$  microbolometers. The TCR in sandwich structures is very high, around  $\alpha = 0.043 \text{ K}^{-1}$ , the current responsivity is in the range of  $R_I = (0.3 - 14) \text{ AW}^{-1}$ , which is around 2 - 3 orders of magnitude larger than that of the boron alloys (a- $\text{Ge}_x\text{Si}_y\text{B}_z\text{:H}$ ) planar structure microbolometers and around 3 - 4 orders of magnitude larger than the intrinsic a- $\text{Ge}_x\text{Si}_y\text{:H}$  film planar structure devices. However the sandwich structure presents a larger current NSD,  $I_{\text{noise}} \approx 10^{-11} \text{ AHz}^{-1/2}$ , which results in a detectivity  $D^* = 4 \times 10^9 \text{ cmHz}^{1/2}\text{W}^{-1}$ .

## 9. Conclusion

Uncooled microbolometers are reaching performance levels which previously only were possible with cooled infrared photon detectors. For uncooled infrared bolometer arrays based on amorphous silicon films the efforts have been conducted to increase the number of pixels included in the arrays, rather than improve the performance characteristics of the microbolometers. Plasma deposited amorphous germanium-silicon (a- $\text{Ge}_x\text{Si}_y\text{:H}$ ) and amorphous germanium-silicon-boron (a- $\text{Ge}_x\text{Si}_y\text{B}_z\text{:H}$ ) used as thermo-sensing films provided a high TCR and, as a consequence, a high responsivity and high detectivity with a improved conductivity. Thus a- $\text{Ge}_x\text{Si}_y\text{:H}$  and a- $\text{Ge}_x\text{Si}_y\text{B}_z\text{:H}$  are very promising materials for its integration on IR detector arrays, and its circuitry in the same chip, avoiding the problems of matching with the input impedance of the electronic circuits. Moreover the manufacture of those devices is aligned with standard CMOS and MEMS foundry processes.

## 10. Acknowledgment

The authors acknowledge: 1. CONACYT for the support for this research through the grant of projects no. D48454-F and 154112. 2. Dr Y. Kudriavtsev from CINVESTAV, Mexico, for SIMS characterization. 3. INAOE, Mexico, for the permission for reproduction of some figures from the Ph.D. thesis work of M. Moreno, titled "Study of IR un-cooled microbolometers arrays based on thin films deposited by plasma".

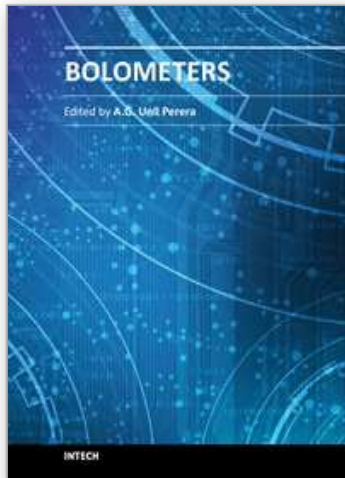
## 11. References

Ambrosio, R.; Torres, A.; Kosarev, A.; Illinski, A.; Zuniga, C.; Abramov, A. (2004). Low frequency plasma deposition and characterization of  $\text{Si}_{1-x}\text{Ge}_x\text{:H:F}$  films, *Journal of Non-crystalline Solids*, Vol. 338-340, pp. 91-96, ISSN 0022-3093.

- Cole, B. E.; Higashi, R. E.; Wood, R. A. (1998). Monolithic Two-Dimensional Arrays of Micromachined Microstructures for Infrared Applications, *Proceedings of the IEEE*, Vol. 86, No. 8, pp. 1679 -1686. ISBN 0018-9219, August, 1998.
- Cole B. E.; Higashi R.E; Wood, R. A. (2000). Micromachined Pixel Arrays Integrated with CMOS for Infrared Applications, *Proceedings of IEEE International Conference on Optical MEMS 2000*, pp. 63 - 64, ISBN 0-7803-6257-8, Kauai, HI, USA, August 2000.
- Delerue, J.; Gaugue, A.; Testé, P.; Caristan, E.; Klisnick, G.; Redon, M.; Kreisler, A. (2003). YBCO Mid-Infrared Bolometer Arrays, *IEEE Transactions on Applied Superconductivity*, Vol. 13, No. 2, pp. 176-179. ISSN 1051-8223.
- Hirota, M.; Morita, S. (1998). Infrared sensors with precisely patterned Au-black absorption layer, *Proceedings of SPIE Infrared Technology and Applications XXIV*, Vol. 3436, pp. 623-634. ISBN 9780819428912, San Diego Ca. USA, July 19-24, 1998.
- Iborra, E.; Clement, M.; Vergara Herrero. L.; Sangrador, J. (2002). IR uncooled bolometers based on amorphous  $\text{Ge}_x\text{Si}_{1-x}\text{O}_y$  on Silicon Micromachined structures, *Journal of Microelectromechanical Systems*, Vol. 11, No. 4, pp. 322- 329. ISSN 1057-7157.
- Kosarev, A.; Moreno, M.; Torres A., Ambrosio R. (2006). Un-cooled micro-bolometer with Sandwiched Thermo-sensing Layer Based on Ge films deposited by Plasma, *Proceedings of Materials Research Society - Amorphous and Polycrystalline Thin-Film Silicon Science and Technology-2006*. Vol. 910, A17-05, ISBN 978-55899-866-7, Warrendale, PA, USA, April 2006.
- Kruse, P. W. (2001). Uncooled thermal Imaging, arrays systems and applications, *Tutorial text in optical engineering*, Volume TT51, SPIE Press, ISBN 9780819441225, Bellingham, Washington USA.
- Moreno, M.; Kosarev, A.; Torres, A.; Ambrosio, R. (2007). Fabrication and Performance Comparison of Planar and Sandwich Structures of Micro-bolometers with Ge Thermo-sensing layer. *Thin solid films*, Vol. 515, pp. 7607-7610, ISSN 0040-6090.
- Moreno, M.; Kosarev, A.; Torres, A.; Ambrosio, R. (2008). Comparison of Three Un-Cooled Micro-Bolometers Configurations Based on Amorphous Silicon-Germanium Thin Films Deposited by Plasma, *Journal of Non Crystalline Solids*, Vol. 354, pp. 2598-2602, ISSN 0022-3093.
- Moreno, M.; Kosarev, A.; Torres, A.; Ambrosio, R.; Garcia, M.; Mireles, J. (2010). Measurements of thermal characteristics in silicon germanium un-cooled micro-bolometers. *Physica Status Solidi C*, C 7, No. 3-4, pp. 1172- 1175, ISSN 1610-1634.
- Pitigala, P.K.D.D.P.; Jayaweera, P.V.V.; Matsik, S.G.; Perera, A.G.U.; Liu H.C. (2011). Highly sensitive GaAs/AlGaAs heterojunction bolometer, *Sensors and Actuators A*, Vol. 167 pp. 245-248, ISSN 0924-4247.
- Rogalski, A. (2003). Infrared detectors: status and trends, *Progress in Quantum Electronics*, Vol. 27, pp. 59-210. ISSN 0079-6727.
- Syllaios, A. J.; Schimert T. R.; Gooch, R. W.; Mc.Cardel, W. L.; Ritchey, B. A.; Tregilgas, J. H. (2000). Amorphous silicon microbolometer technology, *Proceedings of Materials Research Society - Amorphous and Heterogeneous Silicon Thin Films 2000*, Vol. 609, A14.4, ISBN 9781558995178, San Fco. Cal. USA, April, 2000.
- Schaufelbühl, A.; Schneeberger, N.; Münch, U.; Waelti, M.; Paul, O.; Brand, O.; Baltes, H.; Menolfi, C. (2001). Uncooled Low-Cost Thermal Imager Based on Micromachined

- CMOS Integrated Sensor Array, *Journal of Microelectromechanical systems*, Vol. 10, No. 4, pp. 503-510. ISSN 1057-7157.
- Sedky, S.; Fiorini, P.; Caymax, M.; Baert, C.; Hermans L.; Mertens, R. (1998). Characterization of Bolometers Based on Polycrystalline Silicon Germanium Alloys, *IEEE Electron Device Letters*, Vol. 19, No. 10, pp. 376- 378. ISSN 0741-3106.
- Tanaka, A.; Matsumoto, S.; Tsukamoto, N.; Itoh, S.; Chiba, K.; Endoh, T.; Nakazato, A.; Okuyama, K.; Kumazawa, Y.; Hijikawa, M.; Gotoh, H.; Tanaka, T.; Teranishi, N. (1996). Infrared focal plane array incorporating silicon IC process compatible bolometer, *IEEE Transactions on Electron Devices*, Vol. 43, Issue 11, pp. 1844 - 1850, ISSN 0018-9383.
- Takami, H.; Kawatani, K.; Kanki, T.; Tanaka, H. (2011). High Temperature-Coefficient of Resistance at Room Temperature in W-Doped VO<sub>2</sub> Thin Films on Al<sub>2</sub>O<sub>3</sub> Substrate and Their Thickness Dependence, *Japanese Journal of Applied Physics*, Vol. 50, pp. 055804-1 - 055804-3, ISSN 0021-4922.
- Torres, A.; Moreno, M.; Kosarev, A.; Heredia, A. (2008). Thermo-sensing Germanium-Boron-Silicon Films Prepared by Plasma for Un-cooled Micro-bolometers, *Journal of Non Crystalline Solids*, Vol. 354, pp. 2556-2560, ISSN 0022-3093.

IntechOpen



## **Bolometers**

Edited by Prof. Unil Perera

ISBN 978-953-51-0235-9

Hard cover, 196 pages

**Publisher** InTech

**Published online** 09, March, 2012

**Published in print edition** March, 2012

Infrared Detectors and technologies are very important for a wide range of applications, not only for Military but also for various civilian applications. Comparatively fast bolometers can provide large quantities of low cost devices opening up a new era in infrared technologies. This book deals with various aspects of bolometer developments. It covers bolometer material aspects, different types of bolometers, performance limitations, applications and future trends. The chapters in this book will be useful for senior researchers as well as beginning graduate students.

### **How to reference**

In order to correctly reference this scholarly work, feel free to copy and paste the following:

Mario Moreno, Alfonso Torres, Roberto Ambrosio and Andrey Kosarev (2012). Un-Cooled Microbolometers with Amorphous Germanium-Silicon (a-GexSiy:H) Thermo-Sensing Films, Bolometers, Prof. Unil Perera (Ed.), ISBN: 978-953-51-0235-9, InTech, Available from: <http://www.intechopen.com/books/bolometers/un-cooled-microbolometers-with-amorphous-germanium-silicon-a-gexsiy-h-thermo-sensing-films>

**INTECH**  
open science | open minds

### **InTech Europe**

University Campus STeP Ri  
Slavka Krautzeka 83/A  
51000 Rijeka, Croatia  
Phone: +385 (51) 770 447  
Fax: +385 (51) 686 166  
[www.intechopen.com](http://www.intechopen.com)

### **InTech China**

Unit 405, Office Block, Hotel Equatorial Shanghai  
No.65, Yan An Road (West), Shanghai, 200040, China  
中国上海市延安西路65号上海国际贵都大饭店办公楼405单元  
Phone: +86-21-62489820  
Fax: +86-21-62489821

© 2012 The Author(s). Licensee IntechOpen. This is an open access article distributed under the terms of the [Creative Commons Attribution 3.0 License](#), which permits unrestricted use, distribution, and reproduction in any medium, provided the original work is properly cited.

IntechOpen

IntechOpen